Fall 12-2020

Conical Orbital Mechanics: A Rework of Classic Orbit Transfer Mechanics

Cian Anthony Branco
Old Dominion University, cab90@cox.net

CONICAL ORBITAL MECHANICS:

A REWORK OF CLASSIC ORBIT TRANSFER MECHANICS

by

Cian Anthony Branco
B.S.M.E. December 2013, Old Dominion University

A Thesis Submitted to the Faculty of
Old Dominion University in Partial Fulfillment of the
Requirements for the Degree of

MASTER OF SCIENCE

AEROSPACE ENGINEERING

OLD DOMINION UNIVERSITY
December 2020

Approved by:

Prof. Brett Newman (Director)

Prof. Robert Ash (Member)

Prof. Sharan Asundi (Member)

Prof. Dimitrie Popescu (Member)

ABSTRACT

CONICAL ORBITAL MECHANICS:
A REWORK OF CLASSIC ORBIT TRANSFER MECHANICS
Cian A. Branco
Old Dominion University, 2020
Director: Brett Newman

Simple orbital maneuvers obeying Kepler's Laws, when taken with respect to Newton's framework, require considerable time and effort to interpret and understand. Instead of a purely mathematical approach relying on the governing relations, a graphical geometric conceptual representation provides a useful alternative to the physical realities of orbits. Conic sections utilized within the full scope of a modified cone (frustum) were employed to demonstrate and develop a geometric approach to elliptical orbit transformations. The geometric model in-question utilizes the rotation of a plane intersecting the orbital frustum at some angle β (and the change in this angle) in a novel approach to analyze and develop two-body elliptical orbital transformations. Beginning with simple algebraic concepts such as Newton's Second Law and the total specific orbital energy equation, equations combining two-body concepts with more general, Newtonian physics are explored; several equations relating eccentricity directly to a change in orbital energy are developed and applied; and conclusions regarding their importance and usefulness are drawn. Orbital energy exchange, eccentricity, and orbital shape from both inertial and non-inertial perspectives have been developed. Visualizations of transformations are presented throughout to aid in comprehension and clarity. Finally, efficacy of the model, extensions to non-stable orbits, and accuracy and precision with example calculations have been outlined in the Appendices.

ACKNOWLEDGMENTS

To properly acknowledge everyone who has helped me with this thesis would take several pages and likely would not do full justice to their contributions. I would like to especially thank the Graduate Program Director, Dr. Miltos Kotinis, and Department Chair, Dr. Sebastian Bawab for their ongoing help and support throughout the process of writing this thesis. Members of the thesis committee are also due extensive thanks: Dr. Brett Newman for accepting my topic and providing the impetus for my initial investigation; Dr. Robert Ash, PE, for his mentorship and candor for over a decade of schooling; Dr. Sharan Asundi for his assistance with editing and tightening of focus; and Dr. Dimitire Popescu for his perspective, project support, and advice. Finally, I would also like to thank Mrs. Kyndra F. Brown, Developmental Education Director at Tidewater Community College, Chesapeake, for allowing me to write and edit the bulk of this thesis during my time as an Adjunct Professor and Academic Tutor.

This thesis is dedicated to my family, without whose tireless support for my endeavors I would not be here.

TABLE OF CONTENTS

Page

LIST OF FIGURES

Figure Page

CHAPTER 1

INTRODUCTION

1.1 Overview

Modern engineering practice in the instruction of orbital mechanics constitutes an ersatz mix of concepts, frameworks, approaches, and paradigms that are at times needlessly obtuse and opaque. Kepler's Laws, when examined with respect to Newtonian mechanics, quickly become a complex soup of ideas that require considerable time and effort to grasp. Even simple orbital maneuvers such as raising its apsis are often reduced to rows of equations with little regard to what the spacecraft is actually doing. Such an approach need not be standard and would benefit immensely with an injection of new concepts.

The idea of the conic section is fundamental to Keplerian orbital mechanics. In 1605, Kepler[1] realized that the orbit of Mars was in the shape of an ellipse, a conic section. From this discovery, he rapidly concluded that, in fact, any regular orbit about a large mass in space is an ellipse. This concept is fundamentally understood within the realm of orbital mechanics, but the conic itself, the concept of a plane bisecting a cone, is quickly dropped in favor of pure mathematical solutions to Newtonian and Keplerian orbital paths. This view is a mistake; discarding the cone completely ignores the usefulness of the underlying geometry for those with and without experience in orbital mechanics alike.

Within this thesis is discussed a new synthesis of ideas implicit in current orbital mechanics: Conical Orbital Mechanics, often shortened to just Conical Mechanics or just Conic Mechanics. While not new in topic, it offers a different, geometric approach to orbital maneuvers. The focus is kept firmly on stable orbital cases to build the best foundation of understanding and

provide background in concepts already well-understood. Basic maneuvers and transformations are highlighted as well as the unique ability of Conical Mechanics to demonstrate elliptical orbit transformations, a topic Keplerian mechanics often struggles to explain clearly. Limitations to the model are well defined alongside areas of further research. Finally, several examples are presented for review and proof of concept including error comparisons to existing methodologies.

1.2 Literature Review

As a topic area for general research, a conical basis for elliptic orbit transformations is a subject that has little to no background. The areas of orbital transformation and orientation are well established across countless texts but use of a cone as an underpinning idea is essentially non-existent. As-such, a thorough review of existing literature on the subject in a traditional style is almost impossible. Instead, the current approaches for orbital transformations as well as the physical basis for the potential energy perspective are reviewed, to further highlight the complexity existent in the topic at present.

Two books in particular, both Dover publications, are the main areas of review: these are *Fundamentals of Astrodynamics* by Bate, Mueller, and White[2]; and *Introduction to Space Dynamics* by William T. Thomson[3]. Each was only referenced cursorily throughout the development of this thesis, mainly for basic equations, but both are invaluable for development of higher-order, multi-body problems, trajectory analysis, and a better understanding of spacecraft maneuvering. That being said, they are also representative of the current paradigm for orbital mechanics instruction: dense, difficult, and requiring considerable contemplation to fully grasp and appreciate.

Introduction to Space Dynamics[3] devotes considerable effort toward a vector-based analysis of the two-body problem. Firmly rooted in classical dynamics, Thomson's approach begins with the establishment of several coordinate systems and makes extensive use of them through the entire process of formalizing both orbital paths and transformations. The two-body problem is given roughly two pages of coverage, framing it as Newton did, and proceeding to develop much of the rest of the chapter (Chapter 4) from it. While certainly a fantastic reference for the dynamics of spacecraft (heavy emphasis on the dynamics), and certainly in good company with Meriam[4], its usefulness as an introductory course is arguable.

Contrasting *Introduction to Space Dynamics* is *Fundamentals of Astrodynamics*[2] which takes considerable time to develop the conic as a concept, even if its execution does not quite fully utilize the cone. Providing both historical basis, practical applications, and adjacent subject areas (tracking, launch angles, etc.), *Fundamentals* is a more practical book, even if it lacks some of the depth present in *Introduction*. Further, Figure 1.5-2 on page 22 does show a classic, double-cone conic diagram from which the orbital shapes are highlighted. Of course, the authors still drop the cone as soon as it is mentioned in favor of pure mathematical equations, so the reference can only be taken so far. Finally, many of the fundamental equations from literature utilized in Chapters 3 and 4 can also be found in *Fundamentals*, highlighting again its immediate utility despite its shortcomings in the context of this thesis.

1.3 Problem Statement

Classic orbital mechanics relies on several paradigms to simplify orbital maneuvers and provide a better understanding of planetary motion, nominally known as Kepler's Laws. Together, they describe very well the general systems of orbit that can be observed in space. Newton's Laws of gravitation and motion can be added to this framework to develop a very accurate model for

planetary orbital determination. Within this theoretical structure, the concept of the two-body problem, specifically Kepler orbits, can be developed and explored. This concept has been examined extensively in the literature and an exhaustive elaboration will not be given here, but some brief discussion in terms of its limits provides context for the purpose of this thesis.

Kepler orbits as a model of the classic two-body problem are subject to a few limitations. First, all Kepler orbits are regular, which is to say they represent standard conic sections as understood within classic geometry: circle, ellipse, parabola, and hyperbola. Unconventional orbital shapes or continuously varying orbital parameters quickly complicate Keplerian mathematics, and the model is most coherent when the orbits adhere to regular intervals. Second, transformations between orbital shapes require that the impulse or requisite change in velocity occurs over a very small, impulsive time interval relative to the total orbital period, nearly instantaneous. While this assumption holds up very well for conventional chemical propulsion systems, it rapidly degenerates as impulse period grows, or impulse force becomes very small. This breakdown has not been a serious problem thus far as most orbital maneuvers are continuously simulated for higher precision anyway, but many of these techniques are beyond the scope of the two-body framework leaving something to be desired in their execution for understanding and completeness sake. Finally, Kepler orbits, while predicated entirely on conic sections, makes no use of the eponymous cone basis. While an esoteric idea, the lack of a cone is still a fundamental gap in the way this system is often explored and utilized.

The deficiencies are addressed within the scope of this thesis in an effort to better develop, reinforce, and demonstrate a geometric approach to transformations of elliptical orbits based on an analytic conic theory. Each step in the construction of the Conical Mechanics will deal with an explicit concept of the conical transform, starting with framing, and guiding through model

formulation so at the conclusion the full scope of the two-body conical transform may be completely utilized.

1.4 Outline

Chapter 2 is a brief review of elliptical conic sections as they relate to formulation and transformation between types of coordinate systems. In it, the three classic formulations of elliptical conic sections are outlined in addition to setting up the cone implicit in the conic sections, establishing a framing system that is utilized in later chapters. Chapter 3 formalizes the boundary conditions for the model and elaborates on how the model departs from the conic framework devised in Chapter 2. In addition, Chapter 3 introduces the relationship between cone height and specific orbital potential energy, which is essential to the later formulations. Chapter 3 also stipulates the two perspectives in evaluating a spacecraft using the conic transformation: the inertial and non-inertial frames. Chapter 4 begins outlining the numerical work-up of the conic transforms from an inertial perspective. The relationship between the conic transformation angle, β, eccentricity, and specific potential energy is introduced and developed. Chapter 4 also outlines typical stable obit transformations in the energy-height framework.

Chapter 5 builds on the Chapter 4 development moving into the non-inertial frame. Energy-impulse relationships are enumerated, and proper, vehicle-centered orientation is discussed. Chapter 5 also includes a formal definition of the conic transformation angle rate of change, $\dot{\beta}$, as a differential relation between plane angle and specific orbital energy. Finally, Chapter 5 discusses how the conical framework can be integrated with delta-v for maneuver planning. Chapter 6 concludes with a summarization of the development as well as identifying remaining work and limitations to the model. Appendices are included for completeness sake. Appendix I explores how the model may handle unstable orbits initially. Appendix II presents examples of how the conic

model compares to established methodologies for evaluating the two-body problem. Finally, Appendix III contains the MATLAB code used to generate some of the figures contained in the document.

CHAPTER 2

REVIEW OF CONIC SECTIONS

2.1 Overview

With such a strong focus on the concept of the conic section, a brief but thorough review of their scope and mathematical underpinnings will provide context for the discussion going forward. The nature of the conic section has been known since antiquity, and its utility is a well-understood part of elementary and secondary mathematical education. Most existing discourse on conic sections concerns itself with how a three-dimensional, right, circular cone interacts with a two-dimensional coordinate plane, nominally the bisecting plane that generates the conic section. This understanding, while well suited to basic math and the path of an orbiting spacecraft, finds some important relationships beyond just the path in the context of Conic Mechanics; this development is discussed later (Chapter 4). For now, discussion will be confined to a general discourse on the existing understanding of conics, specifically ellipses which are of particular importance to this thesis. The nature of these curves, how they transform, and the different approaches to formulating and quantifying ellipses are all covered.

2.2 Three-Dimensional Conic Section Fundamentals

An ellipse is formed when a right cone is fully bisected by a plane so long as that plane does not intersect the base of the cone. A circle is a special type of ellipse, formed when the plane is parallel to the base of the cone; at any other angle (up to a critical value), the plane will create a true ellipse. Examining the points where the plane and outer surface of the cone intersect creates either the elliptical or circular curve.

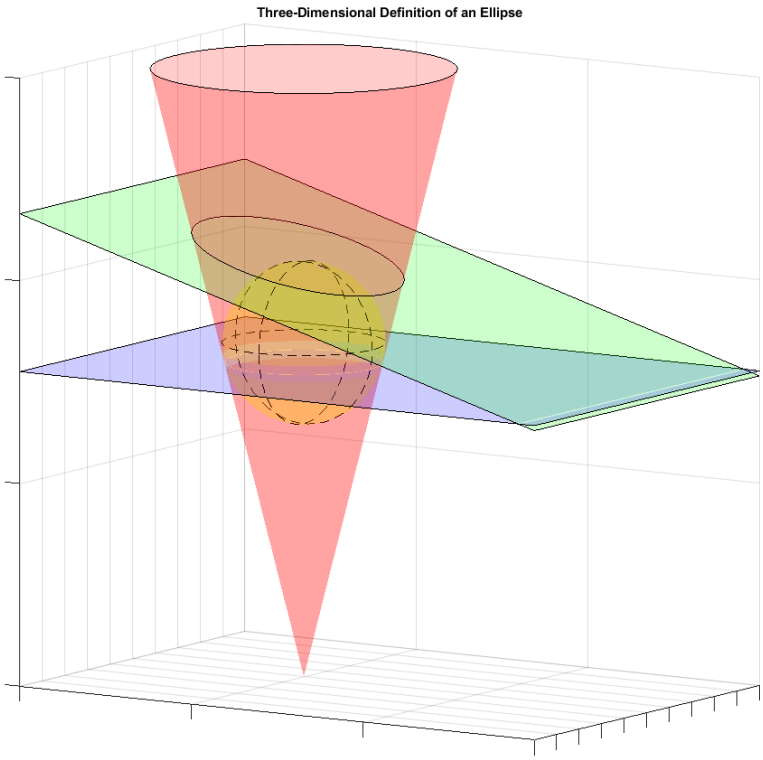

Figure 2-1a Geometric Elliptical Definition

Figure 2-1a illustrates this geometry; it was generated following Figure 8.39 on page 547 of *Calculus and Analytical Geometry* by Thomas[5]. Here, a sphere, inscribed tangent to the cone, also acts to generate the tangent point with the upper plane. The intersect between the upper, tangent plane, and the cone is the ellipse in question. Thomas[5] goes into greater detail on the three-dimensional, directrix-based derivation of eccentricity using this figure, but that is not a consideration in this study. Another helpful source of information on conic geometry was Hass, Weir, and G. Thomas[6].

From Figure 2-1a, a relatively shallow angle produces an ellipse that is nearly circular in shape. As the angle between the two planes increases, the ellipse changes shape, distorting considerably from the original circular shape. At a critical angle, the ellipse becomes another type

of conic section; the parabola, which serves as a boundary case between ellipses (closed-form conic sections) and hyperbolas (open-form conic sections). While parabolas and hyperbolas are not considered in the main body of this thesis, some thought is given to their utility within Conic Mechanics which is briefly addressed in Appendix I. Discussion will instead proceed with proper orientation of the ellipse and different systems of analysis.

2.3 Elliptical Coordinate Systems

To properly analyze an ellipse, a consistent coordinate system was essential. The cone itself served as the fixed reference for the rest of the analysis. The origin will be fixed as the tip of the cone, with the invariant X, Y, and Z axes extending from it. X and Y are fixed parallel to the cone base-plane, while the Z axis is coincident with the cone centerline axis. Figure 2-1b illuminates this representation.

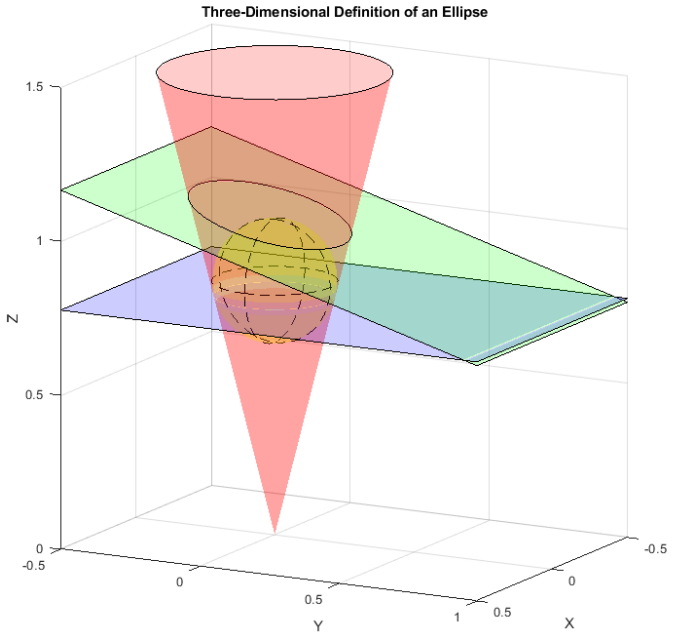

Figure 2-1b Geometric Elliptical Definition with Axes

Note that initial orientation of the cone and invariant axes now becomes arbitrary. The classic methods of analysis can be employed by simply rotating these axes so that the new vertical axis is normal to the point-of-view of the observer, revealing a typical ellipse (Figure 2-2). Specifically, if axes x, y and z are initially aligned with the invariable Y, -X, and Z, and then are rotated about the negative X axis by some amount θ so that z is normal to the bisecting plane, then the relations between the two frames are as follows:

$$x = Y\cos\theta - Z\sin\theta$$

$$y = -X$$

$$z = Y\sin\theta + Z\cos\theta$$

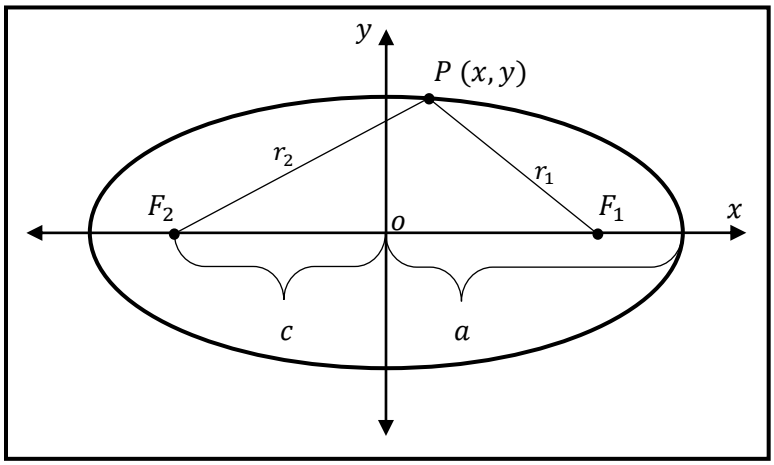

Figure 2-2 Typical Ellipse

Figure 2-2 is composed of many different parts, each of which is described below; some familiarity with the function of each of the parts of the ellipse is assumed herein. The main dimension of the ellipse is defined by the semi-major axis, a, and the focal length, c. Both dimensions, with respect to the origin, O, are used together to define the eccentricity of the ellipse

(more on this in Section 2.4 and Chapter 3). Focal length also describes the position of the foci, F_1 and F_2, with respect to the centered origin. The radius from each of the foci ultimately defines the position, $P(x, y)$, on the elliptical path within a geometric coordinate system. These radii can also be used to convert from geometric to algebraic (or Cartesian) coordinate systems with relative ease. This conversion is also elaborated upon in Section 2.4.

Figure 2-2 will be important throughout this thesis and serves as the fundamental basis for how the cone is reincorporated herein. Elliptic path coordinate system conversions and their significance is covered next. Since the central theme of this thesis is conversion from typical Kepler coordinates to a more geometric, conic system, reviewing the mathematical fundamentals within the simple scope of the ellipse is essential.

2.4 Coordinate System Conversions

An algebraic analysis is the most familiar approach to analyzing ellipses, having been covered thoroughly in the pre-calculus and calculus segments of a standard engineering education. In this format, the ellipse is represented within a Cartesian coordinate plane:

$$\frac{x^2}{a^2} + \frac{y^2}{b^2} = 1 \tag{2-1}$$

where a is equal to the semi-major axis length and b is the semi-minor axis length. Contrasting this is the geometric definition of an ellipse:

$$r_1 + r_2 = 2a \tag{2-2}$$

In Equation (2-2), r_1 and r_2 refer to the distances from each focus of the ellipse to any given point on the curve of the ellipse, with r_1 being equal to the shorter distance of the indicated position *P*, and r_2 the longer distance. The length represented by the sum of the two distances is exactly equal

to twice the semi-major axis length, nominally the "width" of the ellipse. Note that r_1 and r_2 are generalized; depending on the absolute location of point *P*, their respective lengths vary.

Individually these equations describe the ellipse in very different ways, but they are still interconnected. An inspection of the nature of the ellipse even allows for the transformation of one into the other. Such a transform is predicated on the following generalization: for a given non-circular ellipse, r_1 and r_2 will be equal if measuring to either end of the semi-minor axis, as shown in Figure 2-3. In this case:

$$2r_1 = 2a,$$

$$r_1 = a$$

With this relationship, a single quadrant of the ellipse is all that is needed to develop the generalization used to convert representation systems.

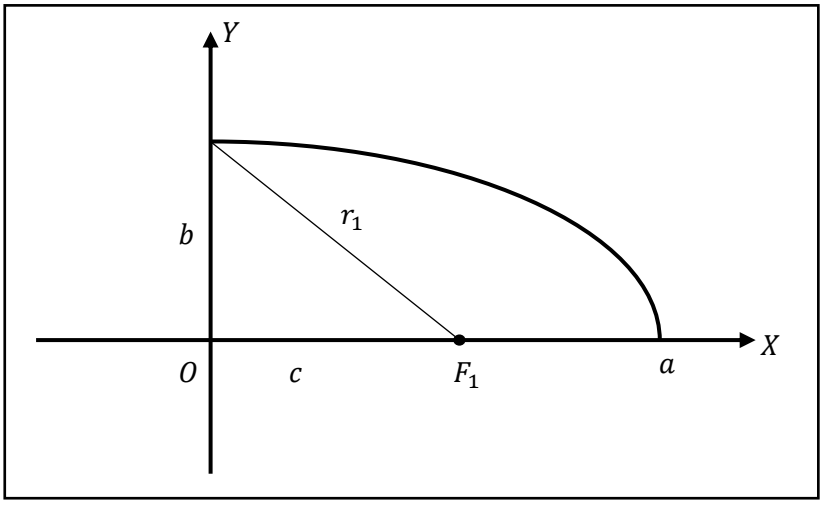

Figure 2-3 Quarter Section of an Ellipse

From Figure 2-3, it is clear that the relation for the semi-minor position can be reduced to a triangular problem, namely the relation between r_1, the semi-minor axis length, b, and the focal length, c. Via Pythagoras;

$$b^2 + c^2 = {r_1}^2$$

$$r_1 = a$$

$$b^2 + c^2 = a^2$$

$$\therefore$$

$$c^2 = a^2 - b^2 \tag{2-3}$$

Equation (2-3) is the main generalization for ellipses: the square of the focal length is always equal to the square of the semi-major axis minus the square of the semi-minor axis. This relation is true regardless of ellipse shape and is critical for the subsequent analysis. With this in mind, an equivalence between the geometric and algebraic formulations can be derived.

Referring again to Figure 2-2, the absolute position *P* is determined from x and y coordinates. By rectifying r_1 and r_2 in terms of x and y, they can be combined with Equation (2-2) and simplified to yield Equation (2-1). First is a basic substitution:

$${r_1}^2 = (x-c)^2 + y^2, \quad {r_2}^2 = (x+c)^2 + y^2$$

These values replace r_1 and r_2 in Equation (2-2). Some algebraic simplification follows:

$$\sqrt{[(x-c)^2 + y^2]} + \sqrt{[(x+c)^2 + y^2]} = 2a$$

$$[(x+c)^2 + y^2] = 4a^2 - 4a\left[\sqrt{(x-c)^2 + y^2}\right] + [(x-c)^2 + y^2]$$

$$(x+c)^2 - (x-c)^2 = 4a^2 - 4a\left[\sqrt{(x-c)^2 + y^2}\right]$$

$$cx - a^2 = -a\left[\sqrt{(x-c)^2 + y^2}\right]$$

$$c^2x^2 + a^4 = a^2x^2 + a^2c^2 + a^2y^2$$

$$a^4 - a^2c^2 = a^2x^2 - c^2x^2 + a^2y^2$$

Recall that $b^2 = a^2 - c^2$ and substitute accordingly:

$$a^2b^2 = x^2b^2 + a^2y^2$$

$$1 = \frac{x^2}{a^2} + \frac{y^2}{b^2}$$

thus leading to the same relation as Equation (2-1).

With just a little basic algebra, Equation (2-1) is converted back into Equation (2-2). While rather obtuse in execution, it nonetheless confirms that the geometric and algebraic perspectives are equivalent: learning one method allows for conversion to the other method and vice versa. However, there are three methods for analyzing ellipses. The conic form is a third form and is the approach used in later chapters; knowing how to convert to it is critically important. While it is possible to convert directly from geometric to conic, only the algebraic to conic conversion will be demonstrated for brevity, leaving an indirect but sufficient geometric-conic relation.

To convert from algebraic to conic forms, two more generalizations of the ellipse are required: eccentricity, *e*:

$$e = \frac{c}{a}$$

and the distance *d* associated with the definition of the directrix of an ellipse:

$$d \equiv \frac{a^2}{c}$$

A directrix is defined as a line outside the area enclosed by the ellipse that provides a fixed reference location when examining points on the ellipse (see Figure 2-4). While the concept of the directrix is essential to understanding the other two major categories of conic sections (parabolas and hyperbolas), it is not generally introduced in discussion of ellipses because they can be defined more easily due to their closed paths. However, because eccentricity is a universal value applicable to any conic section, including the directrix is required for proper analysis and conversion. Note

that although Figure 2-4 shows a single directrix on the right side of the ellipse, there is another on the opposite side with the same distance from the origin.

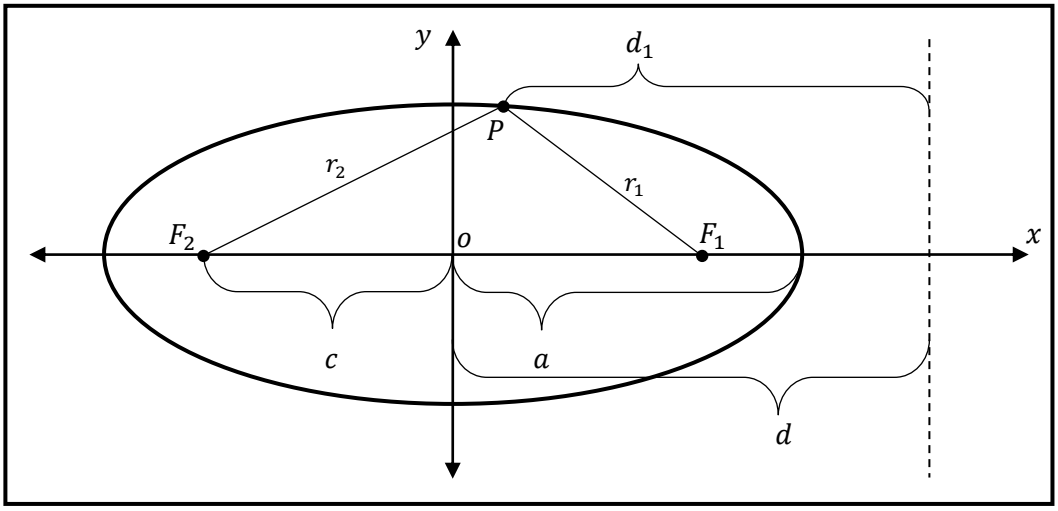

Figure 2-4 Ellipse with Directrix

The directrix and eccentricity concepts are directly related in the conic definition of an ellipse:

$$e = \frac{r_1}{d_1} \tag{2-4}$$

where r_1 is again equal to the shorter, radial distance from the focus F_1 to the indicated position P on the ellipse, and d_1 is the distance from the directrix to that same point. Importantly, the values of d_1 and d are not equal. The distance between the origin and the directrix, d, is constant for a given ellipse, while the distance from the directrix to a point on the ellipse, d_1, varies depending on the actual point. Notably, the value of e is constant for a given ellipse and serves as an important parameter for the analysis of conic sections as a whole. This concept is discussed at length in Chapter 3 but should already be familiar to the reader.

Employing the definitions of the directrix and eccentricity along with Equation (2-4), conversion from algebraic to conic forms can begin. From Equation (2-1), some substitutions are made, recalling that $b^2 = a^2 - c^2$ and $e = \frac{c}{a}$:

$$1 = \frac{x^2}{a^2} + \frac{y^2}{b^2}$$
$$b^2 = \frac{b^2}{a^2}x^2 + y^2$$
$$a^2 - c^2 = [1 - e^2]x^2 + y^2$$

Next, ${r_1}^2 = (x - c)^2 + y^2$, or equivalently $y^2 = {r_1}^2 - (x - c)^2$. Also, $d - d_1 = x$ and $d = \frac{a^2}{c}$, so $x = \frac{a^2}{c} - d_1$:

$$a^2 - c^2 = [1 - e^2]\left(\frac{a^2}{c} - d_1\right)^2 + {r_1}^2 - (x - c)^2$$

Utilizing: $e = \frac{c}{a}$, $ae = c$; thus $\frac{1}{e} = \frac{a}{c}$, after substituting and simplifying, the equation concludes with equivalence to the conic formulation.

$$a^2 = {r_1}^2 - a^2 + 2d_1ae - {d_1}^2e^2 + 2a^2 - 2d_1c$$
$$2a^2 = {r_1}^2 + 2a^2 - {d_1}^2e^2$$
$$(ed_1)^2 = {r_1}^2$$
$$e = \frac{r_1}{d_1} \qquad (2\text{-}4)$$

Finally, Equation (2-4) evolves from the algebra, and the transformation from Cartesian to conic coordinates is concluded. Furthermore, the conversion above implies that the ratio of focal length to semi-major axis is exactly equal to the ratio of radius with respect to the directrix distance. Formally:

$$\frac{r_1}{d_1} = \frac{c}{a} = e$$

As each of these values can be found in any given conic section, the conversion has utility even beyond working with elliptical orbits. Its implications for broader application of the Conic Mechanics (as discussed later) cannot be understated and may prove useful in the future.

2.5 Conclusion

Regardless of perspective or approach, analysis of an ellipse can be carried out and converted from one coordinate system to another utilizing simple equivalencies and minor conversion. Each approach has value with regard to the analysis of the ellipse specifically and conics generally. The focus in Chapter 3, will shift primarily to extensions of Equation (2-4), but conversion to either system can still be accomplished with the methods just outlined. While applications of the Conic Mechanics for parabolas and hyperbolas are only covered in Appendix I, utilization of the analysis and conversions presented in this chapter apply equally well to those cases, despite their deviation from the ellipse.

CHAPTER 3

FRAMING AND BOUNDARIES

3.1 Reference Frames

All classic physics problems are built within the concept of the frame of reference. For Keplerian orbits, the frames of reference can be separated into inertial and non-inertial cases. As the proofs and history behind inertial and non-inertial framing are well-understood concepts, an in-depth investigation is not carried out here. Zipfel[7] provides a thorough development of reference frames, coordinate axes, and their fundamental differences.

Consider a spacecraft in orbit about a large body, the inertial reference frame from the perspective of an observer is the frame that does not appear to be accelerating. The general orbital path of the spacecraft and how it proceeds in its orbit about the nearest celestial body can be treated as the inertial frame; that-is the frame containing the spacecraft, the orbital path, and a planet. In reality, the planet is likely orbiting a local star which, itself, is likely orbiting the center of a local galaxy, and all of these bodies will be subject to gravitational acceleration, so the inertial assumption is only approximate. However, as the focus is on the two-body case initially, an inertial state is an acceptable approximation.

In addition to this inertial frame, another physical frame can be employed for the spacecraft. This frame is non-inertial and can experience accelerations (especially gravity) as it moves about the orbital path. This non-inertial frame is nested within the boundaries of the inertial frame which allows observations of craft from either perspective simultaneously. To elaborate, any orbital transformation will occur due to action of the spacecraft within the non-inertial reference frame, but the net result can only be observed from the perspective of the inertial reference frame. While

Einstein modified the context of these frames by discovering that the inertial assumption was generally an approximation, the errors generated by assuming only a two-body problem with non-curved space-time are relatively small in the context of a typical space mission and can be corrected for missions traversing larger distances. Relativistic effects are not covered in this thesis. The lack of these effects does not diminish the overall utility of the approach, as the velocities involved herein do not approach any appreciable fraction of the speed of light (*c*).

3.2 Model Boundary Conditions

Already present within the inertial frame are a planet and a spacecraft. The planet is assumed to be smooth and airless, with a uniform density and spherical shape. The representative planet mass and radius will match Earth mass (5.9724×10^{24} kg) and equatorial radius (6.3781×10^{6} m). Even though Earth is an oblate spheroid of many layers with a dense atmosphere and variable terrain, to minimize complexity, those details have been ignored. The spacecraft is of arbitrary design with propulsion and attitude orientation systems capable of variable configuration as well as a known center of mass. The craft is assumed to have attained a parking orbit about the planet analogue with a circular orbit in the equatorial plane.

To finalize this system, a brief detour to the realm beyond the inertial frame is required to better define the planet's local environment. As the planet is functioning as an Earth analogue, so it will be assumed the planet is orbiting a star that is a Sol analogue. This star has a mass equal to that of the Sun (1.9885×10^{30} kg), and the planet orbits the star at a distance of 1 Astronomical Unit (AU), or 149,597,870,700 m. Lastly, the planet's orbit will be assumed circular. The actual Earth orbit about the Sun has an eccentricity of only 0.0167. As-such, a circular orbit with a radius of 1 AU is a reasonable approximation.

3.3 Kepler Elements

To formally orient the spacecraft, and by extension the non-inertial frame, within the inertial frame, the six components that comprise the classical orbital elements are employed. These elements, traditionally known as Kepler orbital elements (as shown in Figure 3-1), are the eccentricity (e), semi-major axis (a), inclination (*i*), longitude of the ascending node (Ω), argument of periapsis (ω), and true anomaly (ν) of the orbit. To understand these elements properly, the reference direction (♈) is aligned with a relatively fixed point in the sky with respect to the local center of mass.

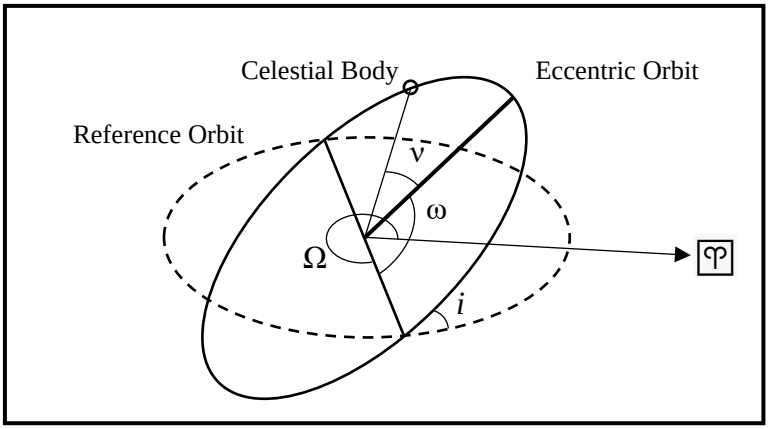

Figure 3-1 Classic Kepler Elements

Initial model calculations assume the spacecraft orbital plane is co-planar with the equatorial plane of the planet (the plane of reference), thus eliminating *i* and Ω. Proper orientation of the spacecraft thus only depends on the argument of periapsis and true anomaly. In conjunction with the semi-major axis length and the eccentricity of the orbit, the spacecraft and non-inertial reference frame can be located within the inertial frame about the planet, requiring as few as four coordinates. Semi-major axis length, and more importantly eccentricity, thus become paramount for inertial frame configurations of the model.

3.4 Eccentricity and Model Overview

As discussed before, all orbits, including ellipses, are forms of conic sections; the key to understanding how orbits are transformed is shaped by and directly affects the eccentricity parameter. Eccentricity is common to all conic sections and by extension, all closed orbits. Denoting a combined value representing the overall "shape" of an orbit, it is a well understood geometric concept that was defined in Chapter 2, but is presented here as a formal equation:

$$e = \frac{c}{a} \tag{3-1}$$

Recall that c is the distance between the center of the conic and one of its foci (focal length), and a is the length of the semi-major axis; the "longer axis" of the ellipse. Ellipses have an eccentricity of less than 1 but greater than zero. A circle is the special case of an ellipse with an eccentricity of zero (the distance between its foci and center being zero since they are one in the same). Parabolas have an eccentricity of exactly 1, while hyperbolas have an eccentricity greater than 1. Eccentricity can be alternatively defined as the ratio of the sines of two angles α and β. These parameters represent the angle between the cone's "slant" and the horizonal axis (for α); and the angle between an intersecting plane and again the horizontal axis (for β) (Figure 3-2):

$$e = \frac{\sin \beta}{\sin \alpha} \tag{3-2}$$

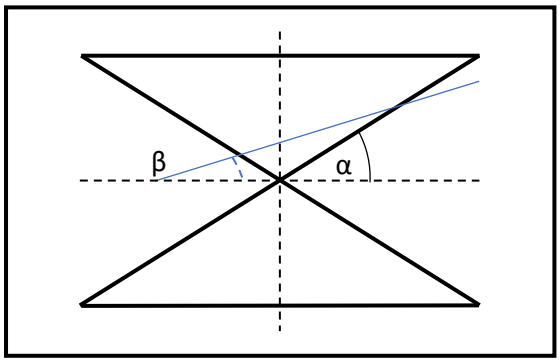

Figure 3-2 Classic Double-Cone Cross-Section

Angle β is denoted as the conic transformation angle and is central to the Conical Mechanics framework. From Chapter 2, ellipses are created when an intersecting plane completely bisects a cone without intersecting the cone tip or cone base. If it is assumed the cone is hollow and infinitely thin, the points of intersection between the cone and the plane constitute an elliptical orbital path. While discussion will be confined to stable orbits, not all elliptical orbits are necessarily stable; a discussion of unstable orbits can be found in Appendix I. This construct makes sense from a mathematical and logical basis, but for some spacecraft orbiting a planet, the nature of the cone is more esoteric.

Narrowing the discussion, just one "cone" representative of all stable orbital paths about the planet, will be considered. This conic boundary is defined as an inverted, right cone with rotated z-axis from Figure 2-2 whose nadir (or tip) is aligned with, but not equal to, the center of mass of the planet (offset between points *o* and F_1 in Figure 2-2). To simplify boundaries, the inverted cone will be further modified into a frustum, that is a cone without a "tip". This lower boundary is a circular sheet with edge exactly equal to the circumference of the Earth analogue and is parallel to the upper boundary, maintaining the property of the frustum being "right"; the surface of the planet or other celestial body physically prevents any orbit from continuing once it reaches the lower boundary; in reality, the spacecraft would crash. Although one could suppose that the tip of the cone may be equal to the body center of mass, this is not correct; the "why" is discussed later. Finally, if the cone "exists" as a means of defining orbital paths, the original vertical axis z representing a spatial property must be replaced with a coincident axis representing some non-spatial quantity. In fact, the vertical axis is energy: specific orbital potential energy. A subtle but important point to emphasize is that the vertically constructed cone is assumed to have sides that expand in a linear fashion.

3.5 Energy Boundaries and Hill Sphere

In classical Newtonian physics, the behavior of a ball tossed into the air is a trivial problem taught to highlight many of the features of Newton's Laws of Motion as well as the effects of gravity. If thrown straight up in the air, the ball, after slowing from initial velocity due to gravity, would eventually reach a maximum altitude with zero velocity. At this zenith, the ball is said to have zero vertical kinetic energy and maximum potential energy, formulated classically as:

$$E_p = mgh \tag{3-3}$$

with potential energy E_p being equal to the mass m of the ball times the local acceleration of gravity g times height h. A trivial concept for sure, but an important one. As a spacecraft gains altitude, it increases its distance from a local source of gravity, consequently increasing its potential energy. Fortunately, the local acceleration due to gravity is not constant, decreasing as a function of the square of the distance from the center of mass. This is Newton's Law of Gravitation, formulated as:

$$F = G\frac{m_1 m_2}{r^2} \tag{3-4}$$

where G is the universal gravitational constant, m_1 and m_2 represent the masses of the two objects under gravitational interaction, r is the distance between the centers of mass of both objects, and F is the magnitude of the force due to gravitational attraction between both objects.

To define the upper boundary of the orbital cone, Newton's equation provides a way to investigate when the example planet's gravity will no longer significantly influence the spacecraft. Respect must be given to the next largest local source of gravity, in this case the Sun analogue defined earlier, to formulate the upper boundary. This restriction is a caveat to the idea the model

is purely two-body, but because it concerns only a boundary, the assumption of two-body mechanics still holds within the model as defined. As a spacecraft continues to modify its orbital path and gain altitude, eventually it will move sufficiently far from the planet that the gravity of the local star will exceed the gravity of the planet. In the case of a spacecraft orbiting Earth, this point is relatively inexact and must factor in numerous parameters including the positions of Luna and Jupiter; for this model, only the planet and its local star are considered.

The concept of a stable orbital region about a celestial body is developed from the concept of the Hill Sphere. Complete formulation of Hill's mathematics can be found in Hill[8]. The Hill Sphere is the region of space bounded by a zero-velocity virtual surface at which the influence of a celestial body and the next closest large source of gravity have equal gravitational attraction. Within the sphere, the gravity of the local body dominates the orbital properties of any object nearby. Consequently, any object within the Hill Sphere of a more massive body will find itself in-orbit about that body. The Moon is within the Hill Sphere of Earth, as are artificial satellites. From Hill's calculations, any object within approximately 1.5 million kilometers of Earth will orbit the planet. Interestingly, this threshold is true for all orbits, including generally unstable ones.

Stable orbits are bounded to a region between one half and one third the radius of the overall Hill Sphere, so placing an upper cone boundary radius of around $5x10^8$ m is a conservative estimate with well-founded physical underpinnings. As a final note: this radius is with respect to the center of mass of the planet. Assuming the planet is analogous to Earth, but spherical, Earth's average equatorial radius of $6.3781x10^6$ m is the radius of the lower bounding circular sheet. Any physical orbital altitude measured with respect to the lower boundary must factor in the average planetary radius to correct for true distance from the planetary center of mass for correct orientation of the focus of a conic section.

3.6 Cone Height

As shown in Equation (3-3), potential energy is a function of spacecraft mass, its height above the planet surface, and the local influence of gravity. While this formulation may appear to create problems with regards to spacecraft mass; local acceleration of gravity rectified at increasing distance from the center; or even an infinite number of cones depending upon the properties of the object in orbit, the model is much simpler: Only one "cone" exists per celestial object. As before, the relevant cone height does not occupy a spatial dimension; instead, the vertical axis for the cone is replaced by energy per unit mass, a notional form of energy-height. This axis reassignment, of course, continues the assumption implicit in Kepler orbits, i.e. that the spacecraft is much less massive than the planet.

Taking the spacecraft and the planet as a system, total energy is defined from the summation of potential and kinetic energy. Potential energy was defined in Equation (3-3), but this formulation is limited in the context of celestial mechanics: as gravity decreases with the square of the distance, a different equation form is needed to take this into account.

$$\epsilon_p = -\frac{GM}{r} \tag{3-5}$$

Equation (3-5) is the specific orbital potential energy equation. Here, ϵ_p is specific orbital potential energy, *G* is the universal gravitational constant, *M* is the mass of the planet (or other larger center of mass), and *r* is the distance between the center of mass of the two objects responsible for gravitational interaction. Note that M is more properly defined as the sum of the mass of both objects, but because the spacecraft is significantly less massive than the planet, its mass is neglected here with negligible error. The specific orbital kinetic energy equation is:

$$\epsilon_k = \frac{v^2}{2} \tag{3-6}$$

where ϵ_k is the specific orbital kinetic energy and v is the orbital velocity. Calculating exact orbital speed can be relatively difficult for non-circular orbits, but the upper and lower bounds of the truncated cone are taken to be circular, the equation becomes trivial:

$$v = \sqrt{\frac{GM}{r}} \tag{3-7}$$

Note that relative speed for a circular orbit is constant and is, in fact, the square-root of the magnitude of its potential energy. Combining Equations (3-5), (3-6), and (3-7) yields the total specific orbital energy equation for ϵ:

$$\epsilon = \epsilon_k + \epsilon_p$$

$$\epsilon = \frac{v^2}{2} - \frac{GM}{r} \tag{3-8}$$

Here the sign for energy is considered negative since the zero-energy reference state is chosen to be at an infinite distance at rest. For circular orbits, total energy is denoted by ϵ_c:

$$\epsilon_c = \frac{GM}{2r} - \frac{GM}{r} = -\frac{GM}{2r} \tag{3-9}$$

Although use of Equation (3-9) for the orbital boundary formulations may be tempting, it would yield several errors. Frustum energy-height is built upon the specific orbital potential energy, not the total energy. If total energy is utilized instead, the calculational error is increased when comparing results to existing methods for determining orbital parameters. As-such, the calculations that follow are based, instead on Equation (3-5). The specific orbital potential energy levels for the frustum boundaries calculations are trivial; only the results are shown. The upper boundary calculation has employed 5×10^8 m as an average radius:

Lower bound, r = Earth Average Radius: $\epsilon = -62.4951 * 10^6 \ \frac{J}{kg}$

Upper bound, r = Hill Sphere Stability Boundary: $\epsilon = -0.7972 * 10^6 \ \frac{J}{kg}$

Limiting bound, r = Hill Sphere Absolute Boundary: $\epsilon = -0.2657 * 10^6 \ \frac{J}{kg}$

Another facet of the upper boundary limitation is now easily observed; namely that specific orbital potential energy is not zero at the upper cone boundary, it is not even zero at the true boundary for the Hill Sphere. In fact, the specific orbital potential energy only approaches zero at the infinite limit, so some approximations need to be made. The process of recalculating an orbit at some predetermined boundary (in this case, the limit of the Hill Sphere), is known as a patched conic method. Patched conics[2] are standard in conventional orbital plots, are a well-understood part of modern celestial mechanics, and are not discussed at length. The only difference is putting the cone back in the patched conic to help make sense of transformations employing a geometric perspective.

To form the frustum, the cone nadir has utilized the average equatorial circumference of the planet, as stated previously. Also, the requirement that the cone nadir could not be considered equal to the center of mass of the planet was stated; the reasoning here comes from Equation (3-9). As radius decreases in Equation (3-9), the average orbital energy increases exponentially. The limit for zero radius is infinite energy, effectively a singularity. Given Earth does not have a black hole at its core, the frustum is formulated instead to side-step the implicit problem resulting from aligning the cone nadir with the center of mass, avoiding that singularity all together. Finally, the singularity is further circumvented by truncating the cone tip thereby restricting possible orbit radii to values only above the Earth analogue radius.

3.7 Conditional Limits, Energy Surface, and Cone Summary

Using the information discussed in Sections 3.1-3.6, Figures 3-3 a and b demonstrate the physical boundary of the frustum. Notice in Figures 3-3a and 3-3b, the circle representing the circumference of the Earth analogue is significantly smaller than the upper boundary circle. This clearly demonstrates why having a lower boundary sheet, rather than a point, does not contribute significantly to error.

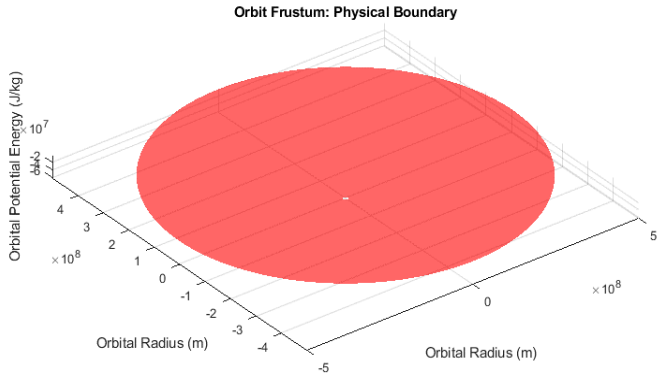

Figure 3-3a Frustum Visualization, Equal Axis Lengths

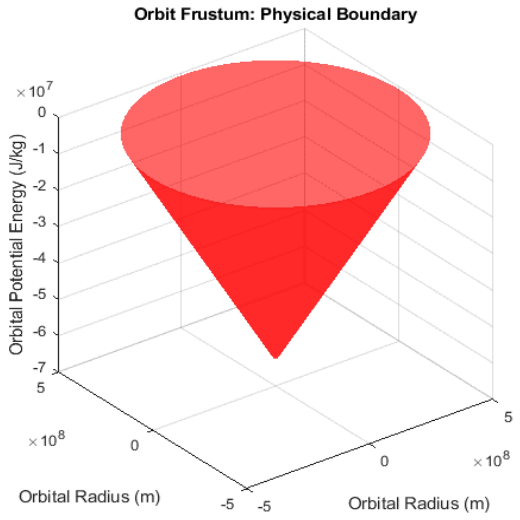

Figure 3-3b Frustum Visualization, Square Axes

To recap: a theoretical “energy frustum” about the smooth, airless, spherical planet has been developed to demonstrate a geometric approach to orbital transformations. The “lower” orbital boundary of the frustrum is equal to the planetary equatorial ring with radius of about 6378 kilometers, and its “upper”, flat boundary is a circle with a radius of approximately half-a-million kilometers. Frustum height between boundaries is defined by subtracting the specific orbital potential energy of the lower bound from that of the upper (stability) bound, yielding an energy-height quantity of approximately 62.4950×10^6 Joules per kilogram. As long as Keplerian assumptions apply, the body-derived gravity is relatively uniform, and relativistic effects do not significantly distort the reference frames, this approach can be used to frame a frustum about any celestial body. With formulation of the boundaries now complete, a proper mechanical analysis can be performed, and the utility of the model can be demonstrated.

In Section 3.4, the eccentricity of an orbit was highlighted as a function of two values, c and a. Eccentricity was also formulated in terms of α and β in Equation (3-2). While β will prove useful as the calculations are carried forward, a closer examination of the frustum will reveal a problem with using the ratio in Equation (3-2) alone, since the vertical spatial axis has been replaced with potential energy. Determination of α relies upon the geometry of a right frustum cross-section: a trapezoid (Figure 3-4).

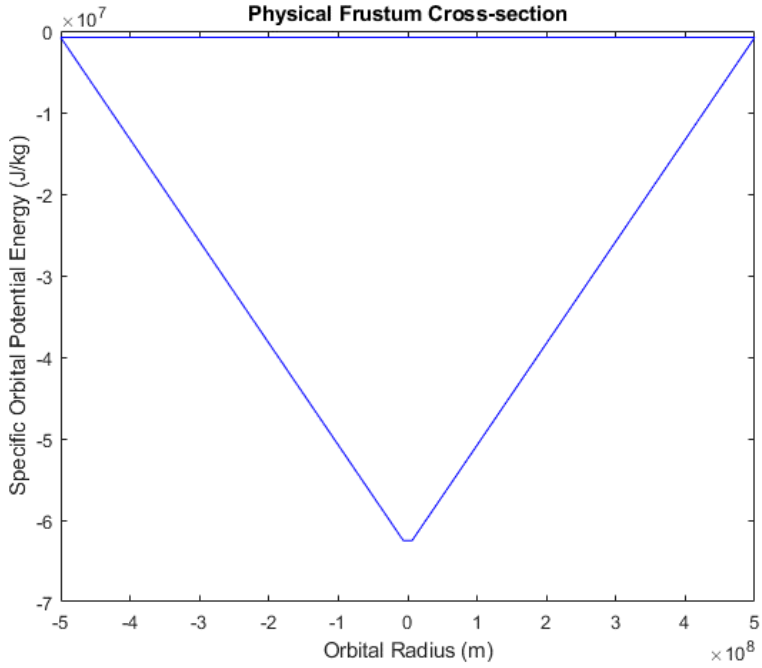

Figure 3-4 Simple Cross-Section of a Frustum: an Exaggerated Trapezoid

Extrapolating from Figure 3-2, α represents the inner angle between the upper surface and a side of the trapezoid. However, attention must be given to the slant sides of the trapezoid. If the vertical axis of the cone is defined as specific orbital potential energy, a differential movement vertically within the cone will yield a change in orbital radius consistent with the specific orbital potential energy equation:

$$\epsilon_p = -\frac{\mu_E}{r} \tag{3-10}$$

For Equation (3-10) (reformulated from Equation (3-5)), G and M, expressed herein as the standard gravitational parameter for Earth, μ_E, are constant, which means that the equation for $\epsilon_p(r)$ cannot be linear, as the trapezoid suggests. Thus, Equation (3-2) cannot be used to define orbital eccentricity directly. Figures 3-5a and 3-5b were generated to provide insight into the cross-section of the nonlinear relationship between orbital radius and energy demonstrating the characteristic bend in angle and constantly shifting slope.

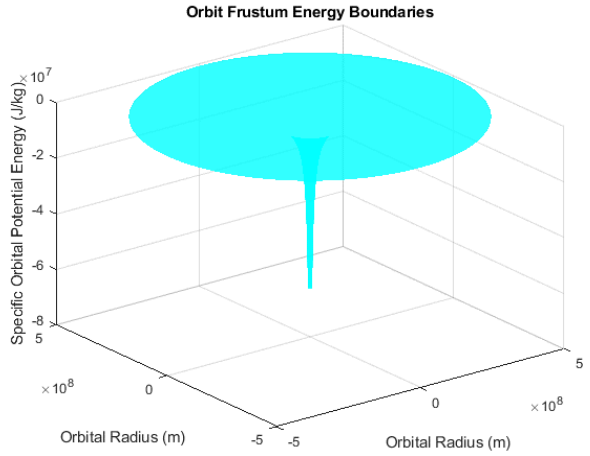

Figure 3-5a Frustum Energy Boundaries

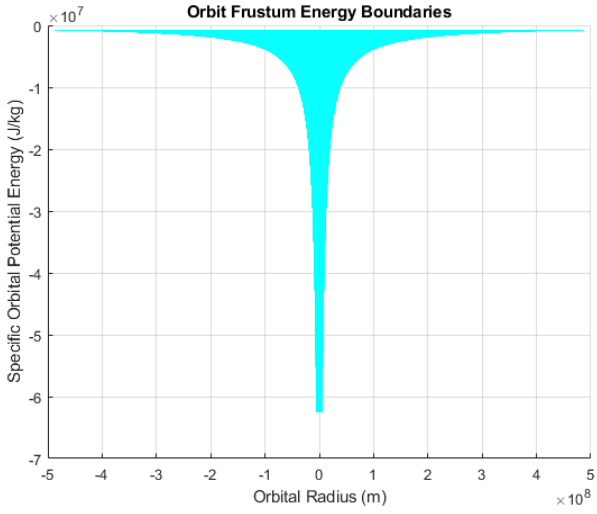

Figure 3-5b Frustum Energy Boundaries, Cross-Section

This information creates a dilemma: Keplerian orbits adhere to an overall shape defined by conic sections with a linear shape, but energy-height dictates that α must be a non-constant value for the non-linear shape from Equation (3-10) to be useful. To resolve this problem, an inspection of conventional orbital mechanics can allow the new formulation to proceed.

Keplerian orbits are defined using a concept known as a “gravity well”. While this idea is a misnomer given gravity applies irrespective of direction; the “shapes” of “gravity wells” very much resemble the shape generated for Figures 3-5a and 3-5b. Under existing paradigms in physics, the overall orbital shape is projected from the upper boundary “down” into the gravity well. This concept leaves much to be desired but does provide a possible solution. Rather than using Figures 3-4 or 3-5 separately, their combination will be employed. Figures 3-6a and 3-6b demonstrate this new shape.

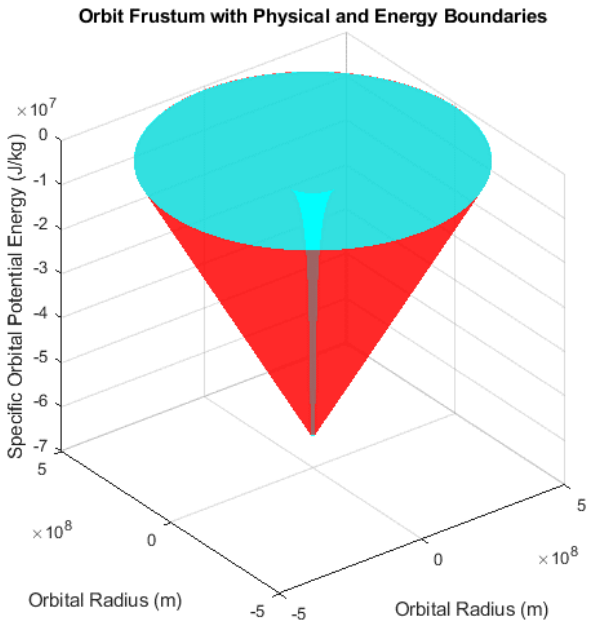

Figure 3-6a Physical and Energy Boundaries Overlaid

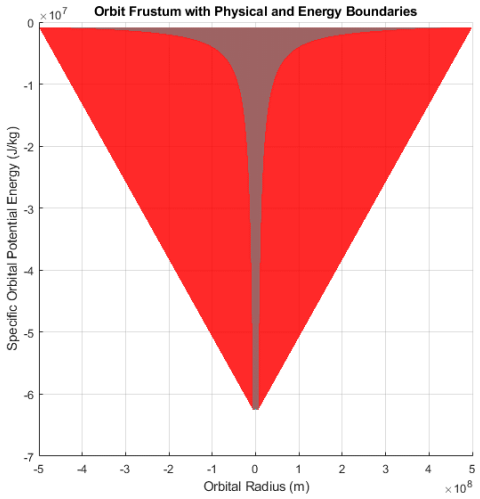

Figure 3-6b Physical and Energy Boundary, Cross-Section

These two figures demonstrate the overall, combined model. As any orbit can be defined as a conic section, an orbit to be investigated simply becomes a plane intersecting the frustum boundary represented by the outer, linear edges. To determine the energy level at any point in that orbit, a vertical projection to the inner construct of orbital potential energy (represented by the nonlinear, curved surface) will be equal to the potential energy at that point in the orbit. In this way, the many different properties of an orbit can be captured in a single, geometric model for rapid comprehension and greater utility.

Here, then, is the orbital cone from patched conics assembled as a single concept. This idea is not new and simply represents a refinement of existing ideas. What is novel is how this assembly can be used for orbital transformations that do not strictly adhere to Keplerian frameworks and simplification of concepts that can be confusing in purely numeric terms. The next chapter will cover the process of transforming established orbits.

CHAPTER 4

INERTIAL REFERENCE FRAME ORBITAL MANEUVERS

4.1 Transformation Outline

In the inertial framework formulation, orbital paths, and the relations between them, are the primary concern. How those transformations occur in terms of the non-inertial spacecraft frame is very important, but the overall orbital shape and its change can be discussed without reference to the behavior of the spacecraft itself. The paradigm set forth in Chapter 2 regarding orientation of the frustum to properly view an orbital path is retained herein and is of paramount importance going forward.

Any object in a fixed, stable orbit above a celestial body is considered to be in a state of continuous motion: it is constantly "falling" towards the center of gravity of the larger body. If its tangential velocity is high enough, then its orbital path never allows it to intersect the surface or atmosphere of the body. In such a stable orbit, the smaller object has several properties: it will always return to the same point in its orbit, it is constantly exchanging potential and kinetic energy, and it sweeps out equal areas under the orbital path in an equal amount of time, i.e. Kepler's 2nd Law.

Essentially, an orbital transformation is a deviation from these steady-state conditions, generally when the smaller object in orbit is subjected to a net force. The origin of the applied force is generally defined in the non-inertial spacecraft frame, but the overall effect is clearly manifest in the inertial frame due to alterations in overall orbital shape and ultimately orbital transformations. While all orbital parameters are potentially affected by these transformations,

eccentricity, and the semi-major have the greatest direct effect on orbital path shape and are of chief concern in the inertial reference frame.

An orbital transformation, and thus orbital maneuvers in general, are driven by the gain or loss of orbital potential and kinetic energy. This relationship between the orbital potential and orbital kinetic energy was highlighted in Equations (3-8) and (3-9) wherein specific orbital energies were summed to total orbital energy. From framing, it was established that the frustum height was defined as specific orbital potential energy.

For any plane that fully bisects the frustum without intersecting the upper or lower boundaries, the "lowest point" of intersection is the periapsis, and the "highest point" is the apoapsis. This can be verified using the curved surface plots from Figures 3-5a and b: by locating the orbital radius at periapsis and apoapsis along the x-axis and tracing lines until they intersect the surface, the intersection points for each line are specific orbital potential energy for each apsis respectively. By subtracting the difference between these two values, the amount of energy exchanged as the spacecraft traverses between periapsis and apoapsis is easily determined. This is the first utility of the frustum: direct measurement of the exchange in specific orbital energy around an orbit. This property is demonstrated schematically in Figure 4-1.

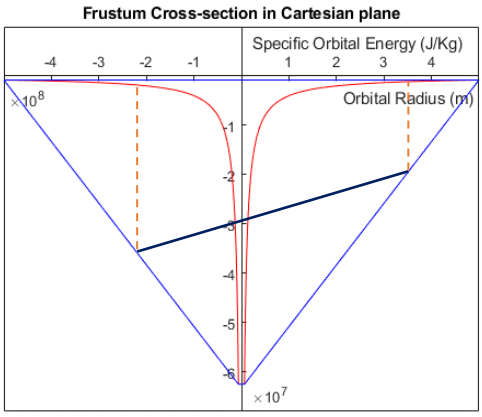

Figure 4-1 Frustum Cross Section with Orbit Plane

To transform the orbit, kinetic energy must be added or removed. The point at which this occurs can produce vastly different orbital shapes depending on several factors confined to the non-inertial frame; for simplicity, the analysis here will be conducted at one of the apses. This approach can be initiated away from the apses employing the frustum approach, but an apses maneuver is easier to describe. When energy is added at an apsis, as the orbit is already at its energetic maximum or minimum, the effect is magnified, thus allowing a clearer picture of how the transform behaves.

4.2 Fundamental Transformation Process

A simple and useful transformation within celestial mechanics is the Hohmann Orbital Transfer[2] which will be employed as an example to demonstrate the conic transform. This type of maneuver is used to transfer a spacecraft from one circular orbit to another employing an elliptical orbit as a go-between. This is accomplished via an impulse at the initial periapsis, followed by a second impulse at the apoapsis of transformed, elliptical orbit, resulting in a second, circular orbit with a larger orbital radius. Such a transformation is easy to demonstrate with the conic model and begins at the periapsis.

Since kinetic energy is already maximized at a periapsis, any increase in kinetic energy will be reflected immediately as an increase in the “altitude” of the apoapsis: because the apoapsis is the point where the maximum exchange of potential and kinetic energy has occurred. Consequently, excess kinetic energy is reflected as an increase in overall potential energy. Such a transformation is known as an apsis-raising maneuver in celestial mechanics and is well defined in the literature. A similar maneuver at the apoapsis, namely gaining kinetic energy, will instead “raise” the altitude of the periapsis: since potential energy is maximized there, any increase in

kinetic energy will raise the overall energy of the orbit, reflected as an increase in periapsis potential energy.

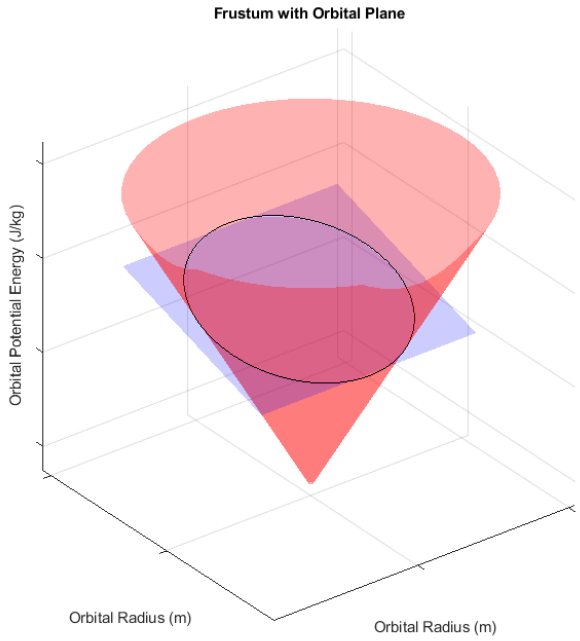

Figure 4-2a Frustum with Orbital Plane

Figure 4-2b Frustum with Orbital Plane in Cross-Section

To transform an orbit using Conical Mechanics, a line parallel to the xy plane can be placed tangent to the outer, slanted boundary of the frustum. In Figure 4-2a, this line would be coincident with the lower edge of the intercepting plane. This line is also coincident with one of the apses of the transfer orbit, in the case of 4-2a, the periapsis. Next, the initial orbital plane is rotated about this line, now the axis of rotation. As the plane is rotated, it will raise or lower the energy levels of all points of the orbit except the tangent point of intersect. In this way, the model reflects observed phenomena in the two-body problem: for any new, stable orbit transformation, the resulting spacecraft orbit will always pass through the original transformation point (in this case, an apsis) as long as no additional transformations are undertaken. The angle rotated through is equal to the quantity $\Delta\beta$ which is equal to the change in angle β from Equation (3-2). This process is highlighted in Figures 4-3 a and b.

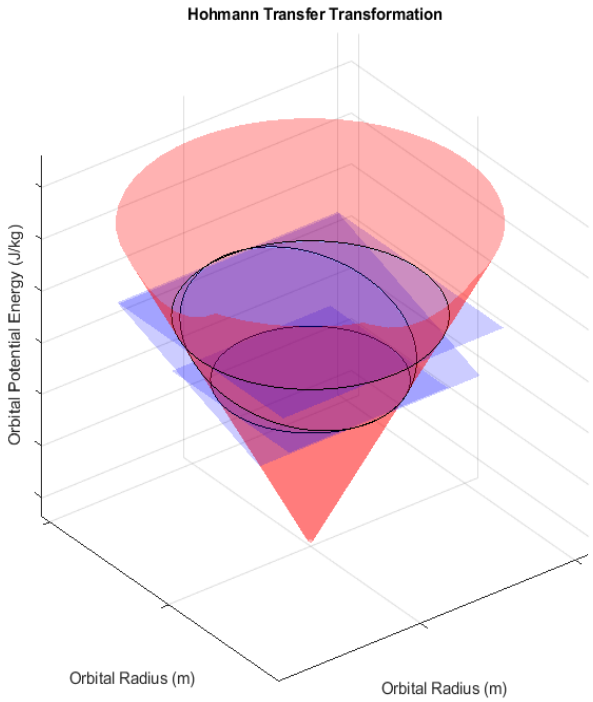

Figure 4-3a Hohmann Transfer Orbit

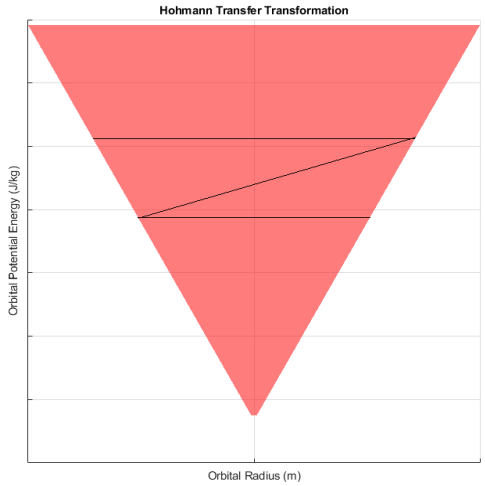

Figure 4-3b Hohmann Transfer Orbit, Side View

Figures 4-3 a and b demonstrate how a typical Hohmann Orbit Transformation can be represented with the cone; from bottom to top, the sequence is as follows: initial circular orbit of $250x10^3$ km; apoapsis raised to $350x10^3$ km producing an elliptical orbit; and finally circularized at $350x10^3$ km. In these figures, the lower plane is rotated about the given axis passing through what becomes the periapsis point for a change in angle β, herein $\Delta\beta$. This generates the second plane in which transforms the initial circular orbit into an elliptical transfer orbit. Once the spacecraft reaches apoapsis on the second plane, the plane is rotated about an axis coincident with the apoapsis (and the plane's upper edge) to circularize the orbit, completing the transfer.

Several things are immediately apparent: the axis of rotation should always be considered positive in the direction of the orbital path; the axis is positive in the orbital direction the spacecraft travels. In addition, the right-hand rule is implemented for sense of direction: counterclockwise rotations about the axis will "raise" an orbit and clockwise rotations will "lower" an orbit. Furthermore, rotations at the apses will always have the greatest immediate effect on orbital path.

Rotational orbit maneuvers elsewhere still adhere to the properties just discussed, but their initial influences are diminished. Finally, the transform is assumed to be instant, in-line with Kepler assumptions, and the magnitude of the transform is equivalent to the magnitude of $\Delta\beta$.

If transforms are represented by changing the angle of the intersecting plane relative to the physical boundaries, then the plane represents a non-spatial synthesis of orbital radius and energy. The value of units in-plane have no meaningful definition. Referring back to Chapter 3, this is why the orbital path is not defined directly by the in-plane points of intersection between the plane and the frustum, but the projection of these points of intersect onto the upper or lower boundary planes; were the points of intersect defined in-plane, their values would be inscrutable.

To ensure a given orbit adheres to basic Keplerian principles, the frustum can again be viewed from directly overhead, eliminating the energy axis and making only the projected orbital paths visible (Figure 4-4).

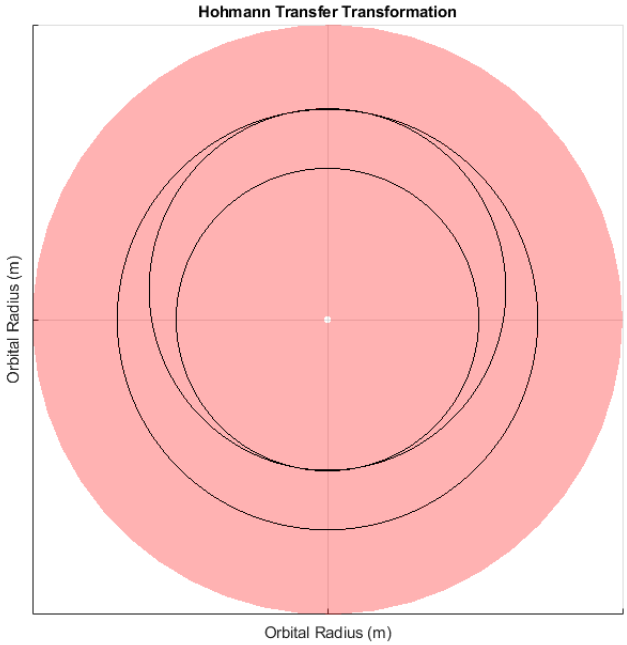

Figure 4-4 Hohmann Transfer Orbit, viewed from x-y perspective

Figure 4-4 clearly demonstrates the classic orbital shapes typically associated with a Hohmann Transfer. Similarly, projection from the boundary intersects to the upper or lower boundary planes will pass through the curved energy surfaces generated via Equation (3-10) (as shown in Figure 4-1), allowing for immediate determination of the orbital energy states as well as their true physical positions. In this way, the model addresses all properties of the orbit simultaneously with easily understood geometric concepts.

4.3 Supporting Equations

Discussion so far has been confined to a general, conceptual idea of how orbits are transformed using the frustum. For the mathematical work of more accurate orbital calculations, initial conditions and limits must be clearly defined. What follows is a work-up of the mathematical model for stable orbits. When the intersecting plane is rotated, the eccentricity of the projected path begins to change. This is due to the change in semi-major axis, *a*, and by extension the change in focal length, c. Any rotation which "raises" the apoapsis will increase the values of a and c, while a rotation which "lowers" the apoapsis will decrease their values. Consequently, any change in *a* is approximately equal to a change in c, more formally:

$$\Delta a = \Delta c$$

Coupled with Equation (3-1), this demonstrates that a change in eccentricity will be proportional to the change in these two orbital parameters. This is also true for a transformation which "raises" or "lowers" the periapsis, but in the reverse sense between the two parameters: a rotation which "raises" the periapsis will increase a but decrease c while "lowering" will decrease a and increase c:

$$\Delta a = -\Delta c$$

To properly transform an orbit, the new orbital eccentricity must be determined based upon the inputs of $\Delta\beta$ and initial orbital radius. β is directly proportional to the orientation of the plane that bisects the frustum with respect to an invariable plane parallel to the upper and lower boundaries (Figure 3-2). The initial β angle for a stable orbit is most easily determined based on the orbit apoapsis and periapsis. Importantly, β is not orbital inclination; conical rotations from a purely physical perspective in which more orbital parameters are affected are not addressed in this thesis.

From Equation (3-2), eccentricity was defined as the ratio of the sines of the planar intersect angle β and the invariable boundary angle α. Determination of α for a given orbital frustum involves comparing the overall energy (height) and difference in orbital radii between the lower and the upper boundaries. Essentially, the side of the cone forms the hypotenuse of a triangle linking the boundary circles, with its vertical leg proportional to the difference in specific orbital potential energy, and a horizontal leg proportional to difference in radii.

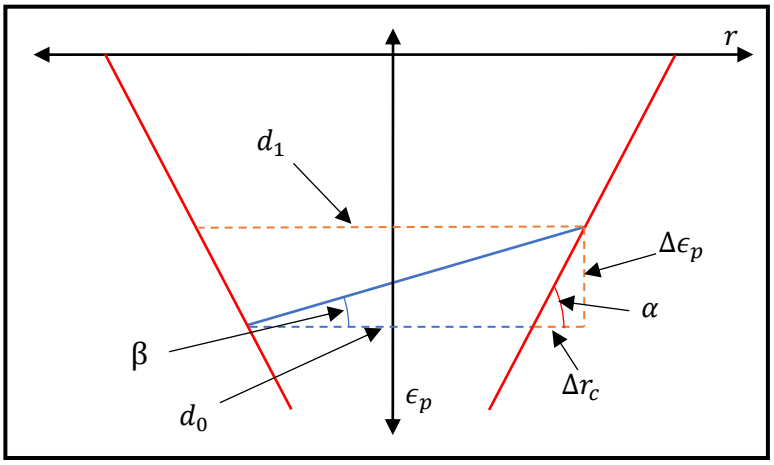

Figure 4-5 Conic Cross-Section with Planar Triangle

Figure 4-5 demonstrates this relationship. Here an initial circular orbit of arbitrary diameter, d_0, has been transformed to an inclined elliptical orbit through some change in angle β; note here the angle is β as the $\Delta\beta$ has already occurred. The difference in radius between the initial

circular orbit and the circular orbit equivalent to the elliptical transfer orbit apoapsis is represented by Δr_c while the difference in specific orbital potential energy between the initial orbit and the apoapsis of the new elliptical orbit is highlighted via $\Delta\epsilon_p$.

To formally determine α:

$$\tan\alpha = \frac{\Delta\epsilon_p}{\Delta r_c} \tag{4-1}$$

Here, the tangent of α is equal to the change in specific orbital potential energy between the top and bottom of the frustum, divided by the change in the equivalent circular orbit radii between the top and bottom boundaries.

Calculating a value for the β of the new orbit (following the $\Delta\beta$) given an initial orbit follows a very similar process. Again using Figure 4-5, the vertical leg is the difference in specific orbital potential energy between the periapsis and apoapsis, and the horizontal leg is equal to the total semi-major axis of the orbit in question (using the projection to invariable planes paradigm discussed earlier). Thus, the tangent of β can be formulated:

$$\tan\beta = \frac{\Delta\epsilon_p}{2a} \tag{4-2}$$

Equation (4-2) is remarkably similar to Equation (4-1), with a notable exception; Equation (4-1) is constant for a given celestial body while Equation (4-2) can change with a particular orbit. Importantly, the value of $\Delta\epsilon_p$ depends on the outer cone boundary values, not the inner, energy surface. As-such, any formulation using (4-2) directly must take this into account. This problem can be avoided by examining the relationship between α and β.

To formulate angle β in terms of α, the change in radius for the specific orbit is compared with the change in outer energy height across the orbit and related via the tangent ratio in much

the same way for α. The difference is the outer energy height cannot be determined using Equation (3-10). As the outer cone boundaries are straight-line boundaries, they do not accurately represent energy: only *projections* from the outer boundary to the inner energy surface properly represents the potential energy at that point. However, because the outer cone angle α was established as constant for any given celestial object, its values can be used in the equation for β. In the calculations that follow, define the orbital diameter, d_{orbit}, as the diameter of a circular orbit with a radius equivalent to the orbital perigee:

$$\tan\beta = \frac{\epsilon_1 - \epsilon_0}{2a}$$

$$2a = d_{orbit} + \Delta r_{orbit}$$

$$\tan\beta = \frac{\Delta\epsilon_{orbit}}{d_{orbit} + \Delta r_{orbit}}$$

$$\tan\alpha = \frac{\Delta\epsilon}{\Delta r} = \frac{\Delta\epsilon_{orbit}}{\Delta r_{orbit}}$$

$$\Delta r_{orbit}(\tan\alpha) = \Delta\epsilon_{orbit}$$

$$\tan\beta = \frac{\Delta r_{orbit}(\tan\alpha)}{d_{orbit} + \Delta r_{orbit}} \tag{4-3}$$

Equation (4-3) is an intermediate step in several derivations in this chapter and Chapter 5 based upon the equations in Chapter 3. With Equations (4-1), (4-3), and (3-2), determination of the eccentricity of any orbit becomes a trivial exercise, expanding the utility of the conic approach. Specific examples of this approach are presented in Appendix II.

4.4 Derivative of β with respect to Energy

Specific orbital potential energy is a fundamental base to this model but isn't always useful when discussing spacecraft maneuvers. As a spacecraft operates by changing its kinetic energy

and thus influencing its overall potential energy, an equation relating a finite change in β (nominally designated $\Delta\beta$ previously) directly to a change in specific orbital energy can be more useful. This is captured employing:

$$\dot{\beta} = \frac{d\beta}{d\epsilon} \tag{4-4}$$

Equation (4-4) relates a differential change in angle β directly to a differential change in total specific orbital energy, while Equations (4-1) and (4-2) only demonstrate a finite change in specific orbital potential energy. To fully realize the expanded form of Equation (4-4), the equations for β, α, and specific orbital energy are all related. Note the continuous, full value for β is considered in the derivation below.

$$\tan\beta = \frac{\epsilon_p - \epsilon_0}{2a}$$

$$\tan\alpha = \frac{\epsilon_p - \epsilon_0}{(r_1 - r_0)}$$

$$\epsilon_p - \epsilon_0 = \tan\alpha\,(r_1 - r_0)$$

$$\tan\beta = \frac{\tan\alpha\,(r_1 - r_0)}{2a}$$

$$\epsilon = -\frac{\mu}{2a}, \qquad 2a = -\frac{\mu}{\epsilon}$$

$$\tan\beta = -\frac{\tan\alpha\,(r_1 - r_0)}{\mu}\epsilon$$

Equation (4-3) becomes critical at this point. That is,

$$\tan\beta = \frac{\Delta r_{orbit}(\tan\alpha)}{d_{orbit} + \Delta r_{orbit}}$$

$$\tan\beta = -\frac{\tan\alpha\,(r_1 - r_0)}{\mu}\epsilon$$

$$\tan\beta = \tan\alpha + \left(\frac{2r_0 \tan\alpha}{\mu}\right)\epsilon$$

$$\tan\beta = \tan\alpha\left[1 + \epsilon\left(\frac{2r_0}{\mu}\right)\right] \quad (4\text{-}5)$$

This is the relation between specific orbital energy and angle β for a given orbital transform at an apsis. The only term that is not a constant is the specific orbital energy, ϵ, meaning the two are directly related with the planar rotations. The derivative of Equation (4-5) (expanded form of Equation (4-4)) follows.

$$\dot{\beta} = \frac{d\beta}{d\epsilon} = \frac{2r_0\mu\tan\alpha}{(\tan^2\alpha)(\mu+2r_0\epsilon)^2+\mu^2} \quad (4\text{-}6)$$

In Equation (4-6), the terms r_0, μ, and α are all constants. Integrating (4-6) for any given change in energy level yields a corresponding change in angle β directly, utilizing the Keplerian approximations. As long as the impulse is instantaneous, Equation (4-6) applies.

CHAPTER 5

NON-INERTIAL FRAME CONSIDERATIONS

5.1 Non-Inertial Frame and Spacecraft Orientation

With the inertial frame perspective and Equation (4-6) fully realized, Chapter 5 examines the non-inertial spacecraft frame including a general overview on proper orientation; energy exchange principles; and a comparison with existing methodologies for working with orbital transformations, including delta-v orbital adjustments.

The non-inertial frame refers specifically to the physical frame of reference centered on the spacecraft. This frame of reference can be considered accelerating; most of these accelerations will come from the spacecraft itself in the form of impulses, but gravitational acceleration must be considered as well. An in-depth discussion of full development of orientation within overlapping frameworks is beyond the scope of this thesis but Bate et. al.[2], Thompson[3], and Meriam[4] all offer excellent insight and further reading. The non-inertial framework here has been developed primarily based on their concepts.

The spacecraft is one element of a two-body system, and the position of its body fixed non-inertial frame is described generally with respect to the more massive object in the system. Again, position of the non-inertial frame within the inertial frame will continue to be described utilizing the common system of orbital elements: eccentricity (e), semi-major axis (a), inclination (i), longitude of the ascending node (Ω), argument of periapsis (ω), and true anomaly (ν) and reference direction (Υ). Eccentricity and semi-major axis are still the main elements.

With the non-inertial frame centered on the spacecraft, a set of XYZ axes (different from that in Chapter 2) is fixed to its center of mass. The X and Y axes of the spacecraft orientation coordinates need only be mutually perpendicular with the third axis, Z, which passes through the center of mass and is parallel with the orbital tangential velocity vector. The absolute position of the X and Y axes is relatively unimportant as long as they maintain a physical frame of reference. Aligning one axis with the radial velocity vector (either the nadir or zenith direction) simplifies spacecraft rotational orientations. Rotations of the craft away from the fixed axes can be expressed with notations common to classical mechanics such as X', Y', and Z'. It is suggested that the Z' axis be parallel to the primary propulsion vector of the craft as the remainder of this model discussion will assume such.

Proper alignment of the axis of rotation for the radius-energy plane can now be outlined. For simplicity, the tangential axis of rotation needs to pass through one of the apses points, as in previous chapters. As long as the tangential axis is co-incident with an apsis, and tangent and co-planar with the orbital path, it will be correctly aligned. Of-course this axis is not some ephemeral mathematical concept, but the Z reference direction of the spacecraft. Alignment of Z, Z', and the axis of rotation are all critical in the next section.

5.2 Orbital Transformations

To transform an orbit, the spacecraft must undergo an impulse. In the physical plane, transformations of orbital parameters occur due to a change in momentum and thus energy. When the spacecraft changes its momentum, it increases its velocity; this in turn raises the total energy of the orbit. For a given impulse lasting a number of seconds, this momentum change corresponds

to a certain change in energy per second. Under classical orbital mechanics, this corresponded to increasing the velocity of the spacecraft at the point of impulse. This increase in kinetic energy corresponds exactly to a change in the energy height of the opposite apsis: “orbit raising”.

The most efficient place to raise/lower an orbit is, again, at the apses where energy is maximized. As the spacecraft proceeds along its orbit, the Z’ axis may be rotated to any orientation. However, aligning Z and Z’ for an impulse at the apses maximizes the resulting change in β. A non-aligned burn here may still result in a change in β, but only from the component of the thrust vector in the Z direction. If all primary conditions are met (apsis, alignment, co-planar, Z and Z’ aligned), calculation of the change in β becomes trivial and utilization of Equation (4-6) is straightforward; the initial maneuver examples below will assume this is the case.

Following the right-hand rule, a prograde burn at periapsis will “raise” the apoapsis. For retro-grade periapsis burns, the apoapsis is instead “lowered”. Intuitively this makes sense as a prograde burn increases kinetic energy while a retrograde burn decreases it. The opposite case is also true where apoapsis, prograde burns “raise” the periapsis and vice versa. Each of these cases constitutes a rotation of the plane intersecting the outer boundaries being rotated about the tangential axis which is, by definition, a change in angle β. This is the link between the non-inertial and inertial frameworks and how action in one reference frame affects the other.

In addition to rotational changes with respect to the outer conical boundary, the energy plot is also affected by changes due to impulse. From the specific orbital energy equation (Equation (3-8) and (3-9)), it was shown that the inner plot’s height directly corresponds to the specific potential energy of an orbit. Recall that the difference in heights between an orbit’s apoapsis and periapsis was directly equal to the amount of energy that transformed between kinetic and potential as the craft proceeded around the orbit.

Because the inner, curved surface deals directly with energy, formulating how an impulse will affect an orbit becomes very easy by examining the inner plot. Estimation (to a high degree of accuracy) of kinetic and potential energies, and consequently velocities, at any point in an orbit can be accomplished simply by comparing the energy height at a given level and working out the difference. Note the fact that a circular orbit with the same radius as a given apsis on a non-circular orbit will, at that point, possess the same specific potential energy as the target orbit, but not the same specific kinetic energy as the target orbit. Again, this makes sense: to transform between orbits, kinetic energy must be gained or lost.

From Equation (3-8), formulation of the total specific orbital energy at the apses and subtracting out the specific orbital potential energy will yield the orbital kinetic energies at each apsis. If, for example, a spacecraft were approaching the periapsis of its orbit, by measuring how much difference in potential energy height there was between the craft's current position and the periapsis, this would correspond directly to the remaining potential energy to be converted to kinetic. Consequently, calculating the craft's current velocity can also be done from the current kinetic energy, as well as its orbital radius and several other orbital parameters. The utility of this approach cannot be understated: simply by examining the cross-section of the energy surface and plotting any orbital position, numerous orbital parameters are yielded simply through direct measurement.

With these details in-mind, formulation of the effect of an impulse on the orbital plane angle (β) should now be obvious. A prograde impulse at periapsis to change a circular orbit into an elliptical orbit will be the first maneuver covered. Again, Z' is aligned with the Z reference direction, and the impulse is assumed to be instantaneous; that is, the impulse begins and completes while the spacecraft is co-incident with the periapsis.

Just before impulse, the orbital path plane and orbital energy planes are both parallel, the initial β angle is equal to zero and the orbital path plane is parallel to the boundary planes. Upon initiation of the impulse, the orbital path plane is rotated about the tangential axis following the right-hand rule. On the opposite side of the circle, the apoapsis begins to rise and the difference between the periapsis' and the new apoapsis' projected heights onto the energy surface are exactly equal to the amount of energy gained during the impulse. The specific orbital kinetic energy total at the periapsis will now be equal to the initial amount plus the amount of kinetic energy added during the impulse. Again, this is directly measurable by comparing the apsis heights in the energy plane.

Moving back from elliptical to circular requires a similar maneuver but in reverse. Again, at the periapsis, instead of the spacecraft pointing along the Z direction (a prograde burn), it will now be aligned so that its primary thruster is pointed in the leading direction, such that Z' is still aligned with Z, but in the opposite direction. This is a retrograde burn and causes opposite rotation of the orbital path plane. Whereas before the rotation occurred counterclockwise, now the rotation will occur clockwise, decreasing apoapsis altitude and energy until the apoapsis and periapsis are again at the same altitude and the orbit returns to circular. Should this burn continue, the rotation about the tangential axis in a clockwise direction would also continue. The point at which the impulse was started now becomes the new apoapsis, while the opposite descending point becomes the new periapsis.

This procedure will work for any stable orbital transformation that occurs at an apsis following this sense: prograde burns will rotate the physical plane in a counterclockwise direction about the tangential axis, retrograde will lead to clockwise. This occurs regardless of the direction of travel of the spacecraft as well. As long as the tangential axis is aligned with Z direction,

prograde (Z' aligned) or retrograde (Z' opposed) will lead to the rotations as described according to the right-hand rule. Successive maneuvers adhering to this paradigm will likewise produce the aforementioned results.

Uncoordinated burns (impulses which occur unaligned with the Z axis) will produce changes in the other orbital parameters besides eccentricity and semi-major axis. The full result of an impulse on all of the orbital parameters is not discussed here. Suffice to say, rectifying the thrust vector components of an impulse to each of the other axes (X and Y) will be key to understanding how this transformation occurs.

5.3 Impulse and $\dot{\beta}$

A general outline for stable orbit maneuvers has now been covered. What follows are the key equations when working with typical elliptical orbital transformations and how they relate to $\dot{\beta}$. As orbital transformations are dependent on a change in the energy level of the current orbit, they are usually accomplished via a series of impulses from the spacecraft's main thruster. An impulse fundamentally changes the spacecraft's momentum resulting in a net energy change which, in turn leads to a change in β and thus an overall change in orbital shape. This process has a few wrinkles.

First, impulse is defined as a known force integrated over a given period of time, classically:

$$J = \int F \, dt$$

Or, for a constant force vector:

$$J = F_{Average}\Delta t \tag{5-1}$$

This analysis will assume the force vector is constant to simplify the calculation. In the case of the spacecraft orbiting the Earth analogue, the force vector is the thrust from the spacecraft's main engine.

Impulse is also exactly equal to the change in the momentum of the spacecraft:

$$J = \Delta p = m_2 V_2 - m_1 V_1$$

This leads to some problems. As a spacecraft expends propellant, its mass will decrease. From the above equation, this means that it takes less force to accomplish the same momentum change for a spacecraft near the end of its useful propellant load as compared with the start. Because of this fluctuating mass profile, a burn for a spacecraft low on fuel will result in a higher $\dot{\beta}$ than for one with a "full tank". In other words, a fixed maneuver thrust value will lead to a variable $\dot{\beta}$, and vice versa. While assuming a fixed mass value would rectify the problem, such an assumption is highly inaccurate for conventional propulsion as reaction mass is usually a significant fraction of vehicle mass for most spacecraft interested in orbital maneuvers.

Thankfully, because impulse is exactly equal to momentum change, determining how impulse affects kinetic energy is relatively straightforward. First, initial momentum of the craft is calculated before the burn. Next, the total impulse of the burn is added to the initial momentum, denoting that a prograde burn will be a positive momentum change while a retrograde burn will result in a negative momentum change. After the burn is complete, final momentum is used to determine the resultant specific kinetic energy change and thus the change in overall orbital shape. While this process does develop a straightforward approach for dealing with impulse and energy, it still abstracts the time component from Equation (5-1), neglecting procession. Some discussion is made regarding procession in Appendix I.

Impulse can also be used to calculate the overall change in the mass of the craft by rewriting the thrust force:

$$F_{Thrust} = \dot{m} \cdot V_e$$

where $\dot{m}$ is equal to mass flow rate, and V_e is the exhaust velocity of the craft's primary propulsion system. Substituting this into Equation (5-1) yields a well-known reformulation of impulse:

$$J = \dot{m} \cdot V_e \cdot \Delta t \tag{5-2}$$

Dividing the total impulse J by V_e yields the total change in mass of the spacecraft for a given orbital maneuver's impulse. Combined with the process discussed previously, this allows for a direct determination of the final velocity for the craft following a burn and thus the ability to calculate the new specific kinetic energy, resulting in the change in orbital shape, etc. While it would be tempting to assume specific kinetic energy could be related to impulse by simply dividing out mass, as the mass value is not constant across the maneuver, this would be highly inaccurate and the change in mass must be accounted for in addition to the change in velocity.

5.4 Comparison to Existing Methodologies

While the conic transform has thus far been underpinned by classic concepts, it still relies on its own terminology and methodologies for determination of orbital shape and thus changes in orbital parameters. Relating a change in β to an existing paradigm would prove helpful in further justifying the conic transform and go some way to ameliorating doubt over its precision. To that end, this section will relate the conic transform, and specifically the change in angle β, to the well-trod concept of delta-v.

Delta-v stands as a corner stone to much of orbital mechanics. Representing a somewhat abstracted concept of the change in velocity required for a given orbital maneuver, it nonetheless finds use at almost all levels of orbital calculation; from simple, two-body mechanics all the way up to and including continual orbital path simulation methodologies. It is especially useful when comparing different approaches for a given maneuver, and even appears in discussion regarding comparison of various propulsion methods. Delta-v is discussed at more length in Bate et. al[2], Thomas[3], and Fortescue[9], so it is assumed the reader will be familiar with the basic idea and formulation for this section to avoid repetition of the finer details.

Under the conditions discussed within Chapter 5, the constant thrust version of delta-v will be used. That is to say delta-v is equal to the magnitude of final velocity minus initial velocity, or:

$$\Delta v = |v_1 - v_0|$$

Change in angle β can be linked to delta-v through total orbital energy in Equations (4-5) or (4-6). As discussed, an impulse will change the specific orbital kinetic energy, ϵ_k, of the spacecraft. By determining ϵ_k before a maneuver and examining the ϵ_k following a maneuver, the overall delta-v is easily determined. Conversely, by treating the delta-v as a change in ϵ_k directly, change in β can, likewise, be examined directly. If the assumptions discussed thus far are held, delta-v may be assumed a change in ϵ_k directly for maneuvers occurring at an apse.

As an aside, delta-v often requires reference to the overall mass of the craft. Discussion of a change in β deals with specific orbital energies, thus neglecting spacecraft mass entirely. Judicious application of the rocket equations and proper momentum calculation will ensure that, though mass exchange is critical for impulses, it does not add error to calculations of change in β. Equation (3-6) related ϵ_k and velocity:

$$\epsilon_k = \frac{v^2}{2}$$

By rearranging the equation, the velocity component can be isolated.

$$v = \sqrt{2\epsilon_k}$$

Taking this formulation and plugging it into the definition for delta-v yields a new equation:

$$\Delta v = \left|\sqrt{2\epsilon_{k_1}} - \sqrt{2\epsilon_{k_0}}\right| \tag{5-3}$$

Equation (5-3) appears complicated, but it does represent something very important: as β was already shown to be a function of specific orbital energy, and the conic model allows for direct measurement of specific orbital potential energy, delta-v and β can be related directly. In addition, due to the instantaneous assumption of thrust duration, the specific orbital potential energy of a given maneuver will be constant for any burn at an apse. As-such, change in specific orbital kinetic energy corresponds directly with change in total specific orbital energy:

$$\Delta\epsilon = \Delta\epsilon_k$$

Equation (4-6) demonstrated the direct relation between change in specific orbital energy and angle β, therefore, any given delta-v can be related directly to a change in beta using existing equations. Formally, this relation is:

$$\Delta v = f(\Delta\epsilon_k) = f(\Delta\epsilon) = f\left(\dot{\beta}\right)$$

The algebraic process to expand this relation is quite complex. As-such, only the required equations and results are shown:

$$\epsilon = \epsilon_p + \epsilon_k$$

$$\Delta v = \left| \sqrt{2\epsilon_{k_1}} - \sqrt{2\epsilon_{k_0}} \right|$$

$$\epsilon_p = -\frac{\mu}{r}$$

$$\tan\beta = \tan\alpha \left[1 + \epsilon \left(\frac{2r_0}{\mu} \right) \right]$$

$$\therefore$$

$$\Delta v = \left| \sqrt{(-\epsilon_p)\left(\frac{\tan\beta_1}{\tan\alpha} + 1 \right)} - \sqrt{(-\epsilon_p)\left(\frac{\tan\beta_0}{\tan\alpha} + 1 \right)} \right|$$

$$\Delta v = \left| \sqrt{(-\epsilon_p)\left(\frac{\tan\beta}{\tan\alpha} + 1 \right)} \right|_{\beta_0}^{\beta_1} \quad (5\text{-}4)$$

In Equation (5-4), both the tangent of α and the specific orbital potential energy values are constant, in-line with the understanding that delta-v can be expressed as a function of angle β alone. Equation (5-4) has a form that is highly reminiscent of the solution to a specific integral, although the form of such a derivative goes beyond the scope of this chapter.

Determination of angle β as a function of delta-v follows a similar process by simply rearranging the delta-v equation and proceeding as before:

$$v_1 = |\Delta v| + v_0$$

$$\epsilon = \epsilon_p + \epsilon_k$$

$$\epsilon_p = -\frac{\mu}{r}$$

$$\tan\beta = \tan\alpha \left[1 + \epsilon \left(\frac{2r_0}{\mu} \right) \right]$$

$$\therefore$$

$$\tan\beta_1 = \tan\alpha\left(\frac{\left(|\Delta v| + \sqrt{(-\epsilon_p)\left(\frac{\tan\beta_0}{\tan\alpha}+1\right)}\right)^2}{(-\epsilon_p)} - 1\right) \tag{5-5}$$

As in Equation (5-4), the specific orbital potential energy and tangent of α are both constant. Therefore, angle β remains purely a function of its initial value (β_0) and the magnitude of the delta-v for the maneuver.

That the change in angle beta can be related to delta-v directly brings the discussion of the conical transformation full-circle. If Kepler assumptions are held, and the required impulse is instantaneous, (5-4) should yield an intelligible answer for any transformation occurring at an apse.

CHAPTER 6

CONCLUSIONS AND FUTURE WORK

Conical Orbital Mechanics has encompassed a more geometric approach to the Kepler two-body problem that has otherwise been overlooked in modern engineering. For stable orbit transformations, a full framework representing spacecraft orientation and elliptical orbit transformations was developed to provide an alternative to the often obtuse and ersatz approach generally involving equations without reference to a geometric model such as a cone. This framework is an extension to the patched conic approach, focused firmly on the cone (or more properly, frustum) to provide a solid grounding from which the mathematical model was derived.

Beginning with the boundaries and limits to the model, the conical mechanics were based on the eccentricity relation within the typical methodologies for evaluating ellipses. Utilizing the cross-section of the orbital frustum representation, angular relationships between conical energy height and planar angle were developed evolving a relation between planar angle and orbital energy. These basic algebraic relations were refined based on the behavior of the spacecraft itself, leading to a differential form of the relation. Further refinements culminating in Equations (5-4) and (5-5) relate the conic transform directly to existing, well-established concepts regarding delta-v management.

The model is self-consistent: fully derivable and invertible subject to the outlined restrictions; the primary challenges develop when these conditions aren't met. Since orbital systems are not actually two-body systems, but are multi-body, actual orbital trajectories are, for lack of a better term, messy. The present model will not necessarily predict a transformation that departs significantly from the two-body case. This is not to say the conical approach cannot be

extended to an n-body case, only that the current formulations do not support it. In addition, the derived equations are based upon orbital transforms about a stable, Earth-mass prototype object with a not-insignificant Hill Sphere. Irregularly shaped primary objects, such as asteroids, or objects lacking uniform density such as Luna, may present a challenge to the exploitation of these equations.

Further, the equations developed throughout rely on a perspective of orbital apsides. If the frustrum model is used for an off-apsis maneuver, it would likely accumulate errors more rapidly. Finally, the transforms have been confined intentionally to elliptical orbits. In-plane orbital adjustments are the most fundamental transform encountered and offering an alternative perspective to traditional methods was the main goal of this thesis. A planar rotational approach to non-stable orbits is entirely feasible but presents challenges that go beyond the general scope of this document.

Ultimately this thesis was an investigation and a starting point; as orbital mechanics is a very well-trod subject area, novel investigations into the subject matter tend not to deal with the fundamentals. While the derivations and examples are rather elementary given the scope of the subject, their utility in providing another way of thinking was the goal. In this vein, extensions of this work go beyond the basic cases and would explore situations and maneuvers more advanced than simply changing the orbital parameters of an ellipse.

One notable problem is the differential form encountered in the following equation:

$$\dot{\beta} = \frac{d\beta}{dt} = \frac{d\beta}{d\epsilon} \cdot \frac{d\epsilon}{dt}$$

$\dot{\beta}$ derived as a change in β over time would offer a true, unique solution to the differential question of how an orbit transforms for a finite impulse maneuver. This is the area where the most progress could be made, since linking the change in specific orbital energy to a finite time interval should be relatively straightforward. Ultimately the Keplerian assumptions limit precise linking of real time to specific orbital energy explicitly because the impulses are assumed to be instantaneous, i.e. Keplerian assumptions, must be modified in order to progress.

While these Kepler-based, two-body, elliptical transformations represent limitations, the approximate model holds up very well. Even though such transformations are quite elementary within the scope of orbital mechanics, some refinement and new examinations, no matter how limited, may yet offer new insights and innovations in the exploration of this vast field.

APPENDIX I

UNSTABLE ORBITS

As discussion has now thoroughly covered the conic transform in the context of stable orbits, unstable orbits will be covered. Unstable orbits can be roughly broken down into 3 major types: degenerate elliptical orbits, hyperbolic orbits, and parabolic orbits. Each is given proper discussion, and some extension of the current equations are also provided. The discussion here is not nearly as detailed as the previous chapters for several reasons but still does justice within the scope of the document.

The unifying principle of all of the unstable orbits is the fact that their orbital plane passes through the upper boundary of the outer stability frustum. As the energy plane could be theoretically extended to infinity, its role is much reduced here, with primary concern given to boundary energy values and total energy required for a given transform as opposed to specific eccentric shifts. That being said, the limitations from the stable cases still apply here, and the Orbital frustum has not been changed.

Degenerate elliptical orbits represent the first category of unstable orbit. Briefly, these are elliptical orbits with an eccentricity very close to, but less than, one whose orbital plane passes through the upper conic boundary. Of further importance is that their β angle value has begun to approach the value of the outer boundary α angle. While still retaining all of the properties of an elliptical orbit, any craft which achieves such an orbit will begin to see all of its orbital parameters change over time.

From Chapter 3, the Hill Sphere was outlined as the area in which all stable orbits can be found. Beyond about 500,000 km from the Earth analogue, orbits can no longer be considered stable. This does not mean a degenerate elliptical orbit (herein known as a DEO) will immediately degenerate as soon as it passes beyond the stability boundary, only that it will accumulate error over time. In-fact, many orbits exist, at least partly, well beyond the 500,000 km theoretical stability limit. However, the equations in Chapters 3 through 5 will not properly describe a DEO that does pass out of the region described by the cone.

Fundamentally, passing beyond the upper boundary essentially takes the problem from two-body to multi-body, requiring considerable simulation or extra measurement and recalculation at each orbit. If the stability equations are to be used in calculating a transformation for or to a DEO, caution is advised, and simulation would be the preferred methodology. Otherwise, DEOs can be treated like other elliptical orbits, with the knowledge that their apoapsis will pass beyond the upper boundary limit.

The level of instability in a DEO is directly proportional to the amount of the orbit that passes beyond the stability boundary. For a DEO with only its apoapsis beyond the stability boundary, it may take several dozen to hundred orbits before error comes up to a detectable level. In contrast, a highly Eccentric DEO with the majority of its orbit beyond the Stability boundary may require constant upkeep, depending upon how its orbit is structured and the other bodies with largest net gravitational pull on it.

Finally, orbits entirely beyond the stability boundary are beyond the scope of this two-body formulation and would need to default to another system. While the orbits of such bodies could be reasonably described under Keplerian assumptions, they will accumulate errors faster than their DEO counterparts. Again, it may require a considerable amount of time before such errors become

detectable, but the fact that local gravity becomes increasingly perturbed by more than one body means the precision of the model will rapidly fail. This all being said, DEOs are still quasi-stable in that any spacecraft with a DEO will still be in orbit around the primary body, in this case the Earth analogue, even after the orbit is perturbed from its original parameters, over a long period of time. Contrasting, hyperbolic and parabolic orbits are both types of escape trajectories that will always take a spacecraft past the upper stability boundary and beyond the local Hill Sphere entirely.

Like the DEOs, both escape trajectory-type orbits pass beyond the upper boundary of the frustum. Unlike the DEO's, the perturbation due to the force of gravity is generally disregarded for a few reasons. First, the model relies on a patched conic concept when moving between local sources of gravity. This requires reformulation of orbital parameters once the spacecraft passes entirely out of the sphere of influence of the original orbit. Second, the amount of time it takes a craft to pass out of the sphere of influence in most non-stellar cases will not lead to an appreciable accumulation of error due to perturbation; a craft will proceed relatively quickly beyond the sphere of influence of most celestial bodies that do no approach stellar mass when placed upon an escape trajectory.

In Chapter 3, the stability boundary was taken from existing literature as a reasonable limit to stability within the framework of the Hill Sphere. In addition, the Hill Sphere was defined as a zero-velocity surface around the local celestial body. Formulating what this means in the context of the model will allow for a greater sense in the development of the hyperbolic and parabolic orbital cases. From Hill's own definition, the true boundary of the sphere is defined with the following equation:

$$r_H \approx a(1-e) \cdot \sqrt[3]{\frac{m}{3M}} \qquad \text{(A-1-1)}$$

Where r_H is the radius of the Hill Sphere, a is the orbit semi-major axis, e is the eccentricity of the orbit, m is the mass of the smaller object, and M is the mass of the larger object. Note that this will calculate the Hill Sphere for the smaller object, not the larger. To determine the Hill Sphere for the Earth analogue, the mass of the Sun and the orbital parameters for the Earth's orbit must be included. Including these yields an r_H of about $1.5*10^6$ km. Any orbit that passes beyond this limit will need to be reformulated into an orbit about the next largest local source of gravity, generally the local star, and in the model case, the Sol analogue. The process for and derivation of patched conics, including Lagrange Points, can be found in Bate et al.[2]; only how the model is used in conjunction with the general approach is covered here.

At the Hill Sphere boundary, depending upon the type of escape trajectory, determination of the orbital parameters for the new orbit will follow a process similar to the one undertaken in Chapters 3 and 4. When the craft leaves the sphere of influence of the local body, its velocity vector and radial distance to the next closest large source of gravity are used to calculate the new orbital parameters for the object. Eccentricity and orbital potential energy will, again, allow the object's orbit to be represented by a plane at some angle β intercepting an energy-height frustum for the new body. The lower boundary will be equivalent the surface or atmosphere of the new center of mass, and the upper boundary becomes equal to the Hill Stability Sphere. Once this occurs, all previously covered material will still apply and transforms, and navigations can be continued as before. As long as the orbital path does not pass beyond the upper boundary, or into the sphere of influence of another object, the conic transform continues to be relevant. This topic has considerably more depth than is discussed here but should be self-evident at this point.

With boundary events now covered, discussion can proceed with hyperbolic orbits. By definition, a hyperbolic orbit is any orbit with an eccentricity greater than 1. From Equation (3-2), hyperbolic orbits must have a β greater than the local α angle. As with the maneuvers for stable orbits, hyperbolic orbits rely on rotations about the Z-tangent axis. Moving from an elliptical, or circular, orbit to a hyperbolic simply involves rotating the path plane about the Z tangent axis past the α angle value. If this rotation is continued until β equals 180°, the top-down perspective on the orbit is that it appears to be a straight line, tangent to the boundary surface and separated by a distance equal to r_1. In this position, the hyperbolic orbit comes to resemble the classic bi-conic hyperbola, even if its physical reality does not reflect the geometric concept.

Hyperbolic orbits have a practical rotational limit of 180°. While the plane could, in theory be rotated past 180°, there is no physical precedent that would allow this: adding more energy when β is equal to 180° simply increases the velocity of the spacecraft and changes the shape of the craft's orbit when it leaves the current Hill Sphere. A closer examination of the existing equations provides more information on how hyperbolic transformations occur.

As with elliptical orbits and DEO's, hyperbolic orbits define their eccentricity with Equations (3-1) and (3-2). Equation (3-2) is key to understanding how the rotational transformation occurs, but Equation (3-1) provides insight into another important hyperbola property: reflectivity. From geometry, the hyperbola is, in-effect, a "double orbit": its shape is symmetric about the center of the orbital shape. The distance between the focus and this center is actually the focal length, c, of the hyperbola. Consequently, the semi-major axis is the distance between the center and the path itself. With Equation (3-1), it is clear why hyperbolas possess an eccentricity greater than 1. To determine semi-major axis length and focal length of a given hyperbolic, parabolic orbits will

be required. As the hyperbolic must always transform from an elliptical to a parabolic first, a few constants found from formulation of the Parabolic will assist in calculation for the hyperbolic.

Parabolic orbits always have an eccentricity equal to 1. This is to say their focal length and semi-major axis are both equal. While this is not technically correct, as a Parabola has no true "center", so the two parameters are equal to infinity, the Parabola does possess a directrix. Recalling from the elliptical formulations that the value r_1 is constant across any rotation, the distance from the periapsis to the directrix is exactly equal to r_1. In fact, for a continuous rotation from elliptical, passing through parabolic, continuing to hyperbolic, r_1 is always constant. This, of course, makes sense under Kepler: the impulse occurs and completes instantly, and the orbit must return to the same point in space from which the impulse was initiated from. If periapsis is constant for a single rotation from stable to unstable, semi-major axis and focal length are determined trivially with the directrix.

The initial position of a hyperbola's center is coincident with the directrix of the parabola that was transformed. This center/directrix lays in the intercept plane itself, is rotated along with the intercept plane about the tangential axis and does not change its position on that plane: only the projection of the center/directrix appears to move. This also means that eccentricity for hyperbolas is still a function of β alone, being readily calculated by simple trigonometry based upon the initial position of the directrix. As rotation proceeds, r_1 must remain constant, so distance from the center of the hyperbola to the periapsis begins to decrease, from the perspective of the physical plane. On the energy surface, β is simply continuing to increase, so the center projection moves closer and closer to the periapsis. When β is equal to 180°, the hyperbola's center and the periapsis appear to overlap, which leads to the eccentricity of a straight line: infinity. The energy

required to achieve this result is absurdly high and generally impractical, but that the concept still reflects general mathematical realities is reassuring.

As far as formulation of hyperbolic energy levels, the previously discussed formulas are all still correct as long as the total orbital specific energy is factored in:

$$\epsilon_{Hyperbolic} = \frac{\mu_E}{2a} \tag{A-1-2}$$

Notice that this energy equation is positive rather than before where the total energy was considered negative. This represents the fact that hyperbolic orbits occur where escape energies are exceeded. Consequently, parabolic orbits, where minimum escape energies are met, has a total orbital specific energy equal to zero. This also means velocity for either of these orbits is just as easy to calculate as the elliptical case: a simple measurement of height for potential energy along the cone and comparison to the total energy will yield the difference in energies which is equal to the kinetic energy, allowing for straightforward calculation of velocity and all of the parameters that follow.

APPENDIX II

SUPPORTING CALCULATIONS

The conic model relies on several paradigms that work together to support the central idea of transformations being rotations or translations of a plane intersecting a frustum. This process is predicated on three major groups of equations from Chapters 3, 4, and 5, all relating back to a change in angle β resulting in orbital path transformations. Examples for each of the major equations discussed in each chapter are presented below for completeness and proof of the efficacy of the equations themselves.

Demonstration that (4-3) is correct within the scope of existing literature is critical to the major calculations present within the thesis. A proof can be devised to demonstrate that β derived from α is still correct. This property is especially useful in the case of a maneuver where only the change in beta is known without reference to the final semi-major axis length (as may be encountered when employing Equation (4-6)). An orbit about the Earth analogue will be used for the proof; here the periapsis is set at 250 km altitude while the apogee is 400 km. All other properties of the model are retained.

The value of α is determined by comparing the upper and lower boundaries for the cone. From Chapter 3, the upper and lower boundary values were outlined:

Lower bound, r = Earth Average Radius: $\epsilon = -62.4951 * 10^6 \ \frac{J}{kg}$

Upper bound, r = Hill Sphere Stability Boundary: $\epsilon = -0.7972 * 10^6 \ \frac{J}{kg}$

Here the average Earth radius at the equator was noted as $6.3781*10^6$ meters, and the Hill Stability Boundary was established as $5*10^8$ meters (with respect to the center of gravity of the planet). Simple trigonometry yields the value for α:

$$\tan\alpha = \frac{\Delta\epsilon}{\Delta r}$$

$$\tan\alpha = \frac{\epsilon_u - \epsilon_l}{r_u - r_l}, \tan\alpha = 0.12499,$$

$$\alpha = 7.1245°, \alpha = .1243\ rad$$

The value of α for the Earth analogue is very shallow, befitting an orbital body with a nominally low mass.

As a known orbit is being investigated, the value for β can be determined two ways and then compared for precision. First, the eccentricity of the orbit will be determined from semimajor axis (a) and focal length (c). Then, β will be computed from Equation (3-2). Finally, (4-3) will be compared to this value for precision.

$$2a = (2 * 6378.1) + 250 + 400 = 13.4062 * 10^6\ m$$

$$a = 6703\ km, c = 75\ km$$

$$e = \frac{c}{a} = 0.01119$$

This eccentricity value is in-line with the type of orbit under consideration: as the orbit is very nearly circular, the eccentricity is likewise very low, as expected. Next, (3-2) is utilized to determine β:

$$e = \frac{\sin\beta}{\sin\alpha}$$

$$\alpha = 7.1245°, \sin\alpha = 0.1240$$

$$0.01119 = \frac{\sin\beta}{0.1240}$$

$$\sin\beta = 1.3876 * 10^{-3}, \beta = 0.07950°, \beta \cong 0.08°$$

Again, following expectation, the value for angle β is very small, befitting an orbit of only minor eccentricity. With an established value for β based upon existing literature, (4-3) can now be verified. The perigee for the example orbit is at 250 km, so the d_{orbit} in the equation will be in reference to that radius:

$$\tan\beta = \frac{\Delta r_{orbit}(\tan\alpha)}{d_{orbit} + \Delta r_{orbit}}$$

$$\Delta r_{orbit} = 400km - 250km = 150\ km$$

$$d_{orbit} = 2(250km + 6378.1km) = 13256.2km$$

$$\tan\beta = \frac{150\ km\ (\tan(7.1245°))}{13406.2\ km}$$

$$\tan\beta = 1.3985 * 10^{-4}, \beta = 0.08013°, \beta \cong 0.08°$$

Both values calculated for β are well within the expected error for engineering calculations, deviating by less than 1%, well within acceptable engineering tolerance.

Having verified Equation (4-3), discussion will now shift to Equation (4-6). Unlike the previous calculations, Equation (4-6) relies on a derivate and subsequent integration to demonstrate its efficacy. Given Equation (4-6) is based upon (4-5), verifying (4-5) first would be useful. The same example orbit from before will be used:

$$\tan\beta = \tan\alpha\left[1 + \epsilon\left(\frac{2r_0}{\mu}\right)\right]$$

$$\epsilon = -\frac{\mu}{2a}, \epsilon = -\frac{3.986 * 10^{14}\ \frac{m^3}{s^2}}{13.4062 * 10^6\ m}, \epsilon \cong -29.733 * 10^6\ \frac{J}{kg}$$

$$r_0 = 6628.1 * 10^3\ m, \tan\alpha = 0.1250$$

$$\tan\beta = 0.1250\left[1 + (-29.733 * 10^6)\left(\frac{2(6628.1 * 10^3)}{3.986 * 10^{14}}\right)\right]$$

$$\tan\beta = 1.3966, \beta = 0.080018°, \beta \cong 0.08°$$

Equation (4-5) is thus verified. To verify Equation (4-6), two scenarios will be used: First, a transformation from a circular orbit of 250 km radius to the example orbit that has been utilized thus far. Second, to show that (4-6) will function irrespective of apsis, Equation (4-6) will be integrated from the apoapsis of an orbit with said apsis at 300 km and periapsis at 250 km. The target orbit in this case will be an orbit with periapsis of 300 km and apoapsis of 400 km. Both cases will compare their $\dot{\beta}$ values to a summed value equivalent.

Aiding in comprehension and ease of calculation, a standard integration will be employed for (4-6), demonstrating only the algebraic portions for proof. The integration is left to the reader to verify independently, but the author has ensured the integral does adhere to proper calculus:

$$\dot{\beta} = \frac{d\beta}{d\epsilon} = \frac{2r_0\mu\tan\alpha}{(\tan^2\alpha)(\mu + 2r_0\epsilon)^2 + \mu^2}$$

$$\int_{\beta_0}^{\beta_1} d\beta = \int_{\epsilon_0}^{\epsilon_1} \frac{2r_0\mu\tan\alpha}{(\tan^2\alpha)(\mu + 2r_0\epsilon)^2 + \mu^2}\, d\epsilon$$

$$\int_{\beta_0}^{\beta_1} d\beta = 2\tan^{-1}\left[\frac{\tan\alpha(\epsilon\, r_0 + \mu)}{\mu}\right]\Bigg|_{\epsilon_0}^{\epsilon_1}$$

$$\Delta\beta = 2\tan^{-1}\left[\tfrac{\tan\alpha(\epsilon_1\, r_0 + \mu)}{\mu}\right] - 2\tan^{-1}\left[\tfrac{\tan\alpha(\epsilon_0\, r_0 + \mu)}{\mu}\right] \qquad \text{(A-2-1)}$$

Equation (A-2-1) will be used for both test cases, itself representing the expanded specific integral of (4-6). The specific orbital energy of the first, circular orbit will be substituted for ϵ_0, while the elliptical orbit's energy will be substituted for ϵ_1. Finally, the r_0 in this equation is equal to the orbital radius of the initial, circular orbit.

$$\epsilon_1 \cong -29.733 * 10^6 \ \frac{J}{kg}$$

$$\epsilon_0 = -\frac{\mu}{2a}, \epsilon_0 = -\frac{3.986 * 10^{14} \ \frac{m^3}{s^2}}{13.2562 * 10^6 \ m}, \epsilon_0 \cong -30.0689 * 10^6 \ \frac{J}{kg}$$

$$r_0 = 6628.1 * 10^3 \ m, \tan\alpha = 0.1250$$

$$\Delta\beta = 7.2324 - 7.1527, \Delta\beta = 0.07972°, \Delta\beta \cong 0.08°$$

What is important to note about this result is that this Δβ is equivalent to the planar angle β for the example 250-400 km orbit from before: recall that β is always measured in reference to a plane parallel to the boundary planes, in this case a plane coincident with the periapsis at 250 km. That a change in β can also be integrated for known energy values and it still yield the expected and correct value further reinforces the efficacy and utility of (4-6). While this exercise may at first appear trivial, it underscores the strength of utilizing equation (4-6) in a situation where only a change in energy is known, ensuring that the change in β calculated will be correct.

To this end, the last example concerning (4-6) will investigate the transformation from one elliptical orbit to another, undergoing an apsis flip in the process; the initial orbit's apoapsis becomes the final orbit's periapsis. As both the initial and final orbits are known, their respective β can be calculated ahead of time to compare to the integrated value yielded by (4-6) to confirm

the calculation is correct. Note that the r_0 for these equations will be equal to the 300 km circular orbit. This is a non-issue for the integration, but the confirmation calculations using (4-5) will have a negative value for β_0. Intuitively this makes sense as the angle is being measured from below the parallel plane and with a plane at the apoapsis of the orbit. Only its magnitude should be used for verification for precision. Much of the calculation herein follows the process demonstrated earlier, and so only the results will be displayed:

Initial Orbit (250 km-300 km): $\epsilon_0 \cong -29.956 * 10^6 \ \frac{J}{kg}$

Final Orbit (300 km-400 km): $\epsilon_1 \cong -29.622 * 10^6 \ \frac{J}{kg}$

$$r_0 = 6678.1 * 10^3 \ m, \tan\alpha = 0.125$$

$$\beta = |\beta_0| + \beta_1 = |-0.02692°| + 0.05323° = \ 0.08015°$$

This value for overall change in β is very similar to the change for the 250-400 km orbit. Again, intuitively this makes sense as the total orbit change is very similar, even though the final orbit only has a β value of 0.05323°. Now to compare this value to the value yielded with (4-6):

$$\Delta\beta = 2\tan^{-1}\left[\frac{\tan\alpha(\epsilon_1 \ r_0 + \mu)}{\mu}\right] - 2\tan^{-1}\left[\frac{\tan\alpha(\epsilon_0 \ r_0 + \mu)}{\mu}\right]$$

$$\Delta\beta = 7.2057 - 7.1259, \Delta\beta = 0.0798°$$

Based upon the similarities between both of these results, that (4-6) is consistent and robust is now self-evident: the error between both results is less than 1%.

A final proof regarding Equation (5-4) is all that remains to be covered. Verification of delta-v poses several extra challenges to the processes discussed thus far, however these are not

insurmountable. As delta-v is nominally the magnitude in the change in velocity of an orbit, it is in reality a measure of the exchange in energy, specifically addition or removal of specific orbital kinetic energy (as per Chapter 5). This knowledge will be used along with the prior orbital transformation to ensure that (5-4) is correct.

Converting a 250 km circular orbit to a 250-400 km elliptical orbit requires a single burn to accomplish. As the circular orbit does not possess apses, the point at which the maneuver is initiated is arbitrary. Recall from Chapter 5 that specific orbital potential energy at the new periapsis will remain constant as the burn will only be introducing kinetic energy. The difference in specific orbital energy between the periapsis and apoapsis corresponds exactly to the excess specific orbital kinetic energy added by the maneuver burn. This comparison can be accomplished several ways: Equation (3-10) will be employed for speed, and the results shown below:

$$\epsilon = -\frac{\mu_E}{2a}$$

$$2a_0 = 13256.2\ km, \epsilon_0 = -30.0689 * 10^6 \frac{J}{kg}$$

$$2a_1 = 13406.2\ km, \epsilon_1 = -29.7325 * 10^6 \frac{J}{kg}$$

$$\Delta\epsilon = \Delta\epsilon_{k_{burn}} = 336.4 \frac{kJ}{kg}$$

This value can then be used with Equation (3-6) to calculate the change in velocity, nominally the delta-v. Initial velocity will correspond to the orbital velocity of the 250 km-radius circular orbit:

$$\Delta\epsilon_k = \frac{v_f^2}{2} - \frac{v_i^2}{2}$$

$$v_i = \sqrt{\frac{\mu}{r}} = 7.7549\ \frac{km}{s}$$

$$336400 = \frac{v_f^2}{2} - \frac{(7.7549 * 10^3)^2}{2}$$

$$v_f = 7.7982\ \frac{km}{s}$$

$$\Delta v = \left|v_f - v_i\right| = 43.3\ \frac{m}{s}$$

A change of about 43.3 m/s is well within reasonable expectation for an orbital maneuver of this type. This delta-v will now be compared with the value yielded by Equation (5-4). Recall that the circular orbit has a β angle of zero, while the β for the final orbit will be taken from prior calculations. In addition, inline with the prior paradigm, the specific orbital potential energy is held at the initial orbital radius (250 km). Finally, note that the specific orbital potential energy in (5-4) is negative, canceling the negative value of the energy as calculated:

$$\Delta v = \left| \sqrt{\left(-\epsilon_p\right)\left(\frac{\tan\beta}{\tan\alpha} + 1\right)} \right|_{\beta_0}^{\beta_1}$$

$$\Delta v = \left| \sqrt{(60.1379 * 10^6)\left(\frac{\tan\beta}{0.062496} + 1\right)} \right|_{0}^{0.08}$$

$$\Delta v = \left| \sqrt{(60.1379 * 10^6)\left(\frac{\tan 0.08}{0.125} + 1\right)} - \sqrt{(60.1379 * 10^6)\left(\frac{\tan 0}{0.125} + 1\right)} \right|$$

$$\Delta v \cong 43.2\ m/s$$

With a percent error of well less than 1%, Equation (5-4) can be supported as correct with a high degree of confidence.

All of the supporting calculations found herein have been verified as much as reasonably possible with existing methodologies and the information is presented as-is for the interested reader. Although the provided examples are simple, the nature of the derivation of each of the equations should allow their broad application within the boundaries of the model quite easily

APPENDIX III

MATLAB CODE

Contained in this Appendix is the raw MATLAB[10] code used to generate some of the visuals found within the body of the document. The code is provided as-is for reference and the curious. MATLAB is a registered trademark of The MathWorks, Inc, Natick, Massachusetts.

```
%Cone with Sphere
figure(1)

%Define Common Variables
Rad=0.2;                                %Sphere Radius
h=1.5;                                  %Cone Height
r=0.375;                                %Cone Upper Circle Radius
del=(Rad*sqrt(r^2+h^2))/(r);            %Variable: Slant Plane/Sphere
orientation
del2=(Rad*h^2)/(r*sqrt(r^2+h^2));       %Variable: Flat Plane orientation

%Define Cone
th=linspace(0,2*pi,21);                 %Memory Allocation
x1=linspace(0,r,21);                    %Memory Allocation
z1=linspace(0,h,21);                    %Memory Allocation
[R,T] = meshgrid(x1,th);                %Memory Allocation
X1 = R.*cos(T) ;                        %Calculate X values
Y1 = R.*sin(T) ;                        %Calculate Y values
Z1=repmat(z1,21,1);                     %Calculate Z values

%Define Cone Upper Circle
thta=linspace(0,2*pi,50);               %Define Theta
Xc=r*cos(thta);                         %Calculate X values
Yc=r*sin(thta);                         %Calculate Y values
Zc=1.5*ones(1,50);                      %Calculate Z values

%Define Sphere
[X,Y,Z]=sphere;                         %Define Sphere
X2=X*Rad;                               %Calculate X values
Y2=Y*Rad;                               %Calculate Y values
Z2=Z*Rad;                               %Calculate Z values

%Define Sphere circles
%Horizontal
Xs1=Rad*cos(thta);                      %Calculate X values
Ys1=Rad*sin(thta);                      %Calculate Y values
Zs1=del*ones(1,50);                     %Calculate Z values
%Vertical YZ
Xs2= zeros(1,50);                       %Calculate X values
Ys2=(Rad*sin(thta));                    %Calculate Y values
Zs2=(Rad*cos(thta))+del;                %Calculate Z values
```

```
%Vertical XZ
Xs3=(Rad*cos(thta));                    %Calculate X values
Ys3=zeros(1,50);                        %Calculate Y values
Zs3=(Rad*sin(thta))+del;                %Calculate Z values


%Define Flat Plane
X3=linspace(-0.5,0.5,2);                %Calculate X values
Y3=linspace(-0.5,1,2);                  %Calculate Y values
Z3=ones(2).*del2;                       %Calculate Z values

%Define Slanted Plane
thet=75;                                %Plane Angle
dy=Rad*cosd(thet);                      %Change in y
dz=Rad*sind(thet);                      %Change in x
m=tand(thet-90);                        %Slope
yint=-(m*dy)+(del+dz);                  %Y Interval
zlim1=((-0.5)*m)+yint;                  %Z limit
zlim2=((1)*m)+yint;                     %Z limit
X4=linspace(-0.5,0.5,2);                %Calculate X values
Y4=linspace(-0.5,1,2);                  %Calculate Y values
z4=linspace(zlim1,zlim2,2);             %Calculate Z values
z4=z4';                                 %Calculate Z values
Z4=repelem(z4,1,2);                     %Calculate Z values

%Define Cone/Slant Plane Intercept Ellipse
P1=[X4(2),Y4(1),Z4(1,2)];               %Memory Allocation
P2=[X4(1),Y4(2),Z4(2,1)];               %Memory Allocation
P3=[X4(1),Y4(1),Z4(1,1)];               %Memory Allocation
V1=P3-P1;                               %Vector Definition 1
V2=P2-P1;                               %Vector Definition 2
Coeff=cross(V1,V2);                     %Cross Product
d=dot(Coeff,P1);                        %Dot Product
Coeff=[Coeff,d];                        %Lump Coefficient
[X5,Y5]=meshgrid(linspace(-0.5,0.5));   %X & Y allocated
ZCone=sqrt(X5.^2+Y5.^2)./(r/h);         %Cone Z values constraint
Zplane=(Coeff(4)-((Coeff(1)).*(X5))-((Coeff(2)).*Y5))./(Coeff(3));%Plane Z
values constrained
ZDiff=ZCone-Zplane;                     %Cone-Plane difference
ECont= contours(X5, Y5, ZDiff, [0 0]);  %Contour Values
X5L = ECont(1, 2:end);                  %Calculate X Values
Y5L = ECont(2, 2:end);                  %Calculate Y Values
Z5L = interp2(X5, Y5, ZCone, X5L, Y5L); %Calculate Z Values

%Plot All Sub-figures
Cone=surf(X1,Y1,Z1); hold on            %Define Cone
plot3(Xc,Yc,Zc,'- k');                  %Plot Cone
Sph=surf(X2,Y2,Z2+(del));               %Plot Sphere
plot3(Xs1,Ys1,Zs1,'-- k');              %Plot Sphere circle Horizontal
plot3(Xs2,Ys2,Zs2,'-- k');              %Plot Sphere circle Vertical YZ
plot3(Xs3,Ys3,Zs3,'-- k');              %Plot Sphere circle Vertical XZ
Plane1=surf(X3,Y3,Z3);                  %Plot Flat Plane
Plane2=surf(X4,Y4,Z4);                  %Plot Inclined Plane
line(X5L, Y5L, Z5L, 'Color', 'k', 'LineWidth', 1);%Plot Intercept Circle

%Set Parameters
```

```
set(Cone,'FaceColor','r','FaceAlpha',0.2,'EdgeColor','none')
set(Sph,'FaceColor','y','FaceAlpha',0.2,'EdgeColor','none')
set(Plane1,'FaceColor','b','FaceAlpha',0.2,'EdgeColor','k')
set(Plane2,'FaceColor','g','FaceAlpha',0.2,'EdgeColor','k')

%Format Figure
title('Three-Dimensional Definition of an Ellipse')
%xlabel 'x'
%ylabel 'y'
%zlabel 'z'
xticklabels([])
yticklabels([])
zticklabels([])
axis equal
hold off
```

BIBLIOGRAPHY

1. Koestler, A., *The Watershed: A Biography of Johannes Kepler*, Anchor Books Doubleday & Company, Garden City, New York, 1960.

2. Bate, R.E., Mueller, D. D., and White, J. E., *Fundamentals of Astrodynamics*, Dover Publishing Inc, Mineola, New York, 1971.

3. Thomson, William T., *Introduction to Space Dynamics*, Dover Publishing Inc, Mineola, New York, 1986.

4. Meriam, J. L., *Dynamics, Second Edition, S.I. Version*, John Wiley & Sons, Ltd., New York, 1975.

5. Thomas, G. B. and Finney, R.L., *Calculus and Analytical Geometry*, Addison-Wesley Publishing, Reading Massachusetts, 1984.

6. Hass, J., Weir, M. D., and Thomas, G. B., *University Calculus*, Pearson, Boston Massachusetts, 2007.

7. Zipfel, Peter H., *Modeling and Simulation of Aerospace Vehicle Dynamics, Third Edition,* American Institute of Aeronautics and Astronautics, Reston, Virginia, 2014.

8. F ortescue, P., Swinerd, G., and Stark, J., *Space Craft Systems Engineering, Fourth Edition*, John Wiley & Sons, Ltd., Chichester, West Sussex, United Kingdom, 2011.

9. MATLAB. (2019). version 9.4.0.813654 (R2018a). Natick, Massachusetts: The MathWorks Inc.

Note: Earth and Solar masses, Specific Gravitational Parameters for Earth, and other celestial constants found within this document obtained from public web pages of the National Air and Space Administration via NASA.gov. General equations present throughout which may be found in works listed in the Bibliography remain the property of their respective authors or as otherwise referenced there-in.

VITA

Cian Anthony Branco

EDUCATION

Master of Science in Aerospace Engineering, Department of Mechanical and Aerospace Engineering, Old Dominion University, Norfolk, Va. 2015-2020

Thesis Topic: “Conical Orbital Mechanics: A Rework of Classic Orbit Transfer Mechanics”

Bachelor of Science in Mechanical Engineering, Department of Mechanical and Aerospace Engineering, Old Dominion University, Norfolk, Va., 2009-2013

ACADEMIC EMPLOYMENT

Adjunct Professor of Mathematics and Academic Tutor, Tidewater Community College, Chesapeake, Va. 2015-2019

Responsibilities include: Instruction of remedial and introductory courses in mathematics to meet college-wide standards from math proficiency. Additionally, provided tutoring in subject areas encompassing the foundations underpinning most science degrees including introductory university physics; calculus and differential equations; introductory university chemistry; and topics relating to undergraduate mechanical engineering courses.